ORIGINAL ARTICLE

Multimodal study of the neural sources of error monitoring in adolescents and adults

Stefania Conte[1] | John E. Richards[1] | Nathan A. Fox[2] | Emilio A. Valadez[2] | Marco McSweeney[2] | Enda Tan[2] | Daniel S. Pine[3] | Anderson M. Winkler[3] | Lucrezia Liuzzi[3] | Elise M. Cardinale[3] | Lauren K. White[4] | George A. Buzzell[5]

[1]Department of Psychology, University of South Carolina, Columbia, South Carolina, USA

[2]Department of Human Development and Quantitative Methodology, University of Maryland, College Park, Maryland, USA

[3]National Institute of Mental Health, Emotion and Development Branch, Bethesda, Maryland, USA

[4]Lifespan Brain Institute of the Children's Hospital of Philadelphia and Penn Medicine, Philadelphia, Pennsylvania, USA

[5]Florida International University and the Center for Children and Families, Miami, Florida, USA

Correspondence
Stefania Conte, Department of Psychology, the State Univeristy of New York (SUNY), Binghamton, NY, USA.
Email: sconte@bighamton.edu

Funding information
Eunice Kennedy Shriver National Institute of Child Health and Human Development, Grant/Award Number: R01HD18942; National Institute of Mental Health, Grant/Award Number: U01MH093349 and ZIAMH002782

Abstract

The ability to monitor performance during a goal-directed behavior differs among children and adults in ways that can be measured with several tasks and techniques. As well, recent work has shown that individual differences in error monitoring moderate temperamental risk for anxiety and that this moderation changes with age. We investigated age differences in neural responses linked to performance monitoring using a multimodal approach. The approach combined functional MRI and source localization of event-related potentials (ERPs) in 12-year-old, 15-year-old, and adult participants. Neural generators of two components related to performance and error monitoring, the N2 and ERN, lay within specific areas of fMRI clusters. Whereas correlates of the N2 component appeared similar across age groups, age-related differences manifested in the location of the generators of the ERN component. The dorsal anterior cingulate cortex (dACC) was the predominant source location for the 12-year-old group; this area manifested posteriorly for the 15-year-old and adult groups. A fMRI-based ROI analysis confirmed this pattern of activity. These results suggest that changes in the underlying neural mechanisms are related to developmental changes in performance monitoring.

KEYWORDS
adolescents, decision-making, ERN, ERP, flanker task, fMRI

1 | INTRODUCTION

The ability to monitor performance influences human behavior by detecting events, actions, or environments where additional control over behavior may be required. Individual variation in these skills relates to cognitive processes such as stimulus encoding, response selection and execution, response evaluation. These skills and the

associated brain function have a protracted developmental time course, and individual differences which may be related to the onset of certain forms of psychopathology. However, little multimodal imaging has examined age differences in neural generators underlying performance and error monitoring. It is important to augment developmental research on behavior by measuring neural generators, which may be more sensitive markers of underlying processes linked to psychopathology (Moser et al., 2013). Remnants of neural maturation during the first years of life manifest throughout adolescent development. In fact, complex cognitive abilities arising in adolescence can reflect these earlier remnants. This creates opportunities for new skill development and vulnerability for psychiatric symptomatology. Therefore, adolescence can be characterized by sensitive periods particularly for high-level cognitive processes (Fuhrmann et al., 2015; Sydnor et al., 2021). Studies in basic science examining such high-level cognition localize the neural generators of behavior to particular brain regions (Erickson et al., 2005; vel Grajewska et al., 2011). Attempts to extend such basic science research to youth benefit from studies that can localize the neural generators of clinically relevant phenomena. Prior research suggests that brain changes support maturing adaptive behaviors among healthy adolescents and that such changes could trigger atypical behaviors and lead to the development of mental disorders. Research on the neural response to errors could elucidate features of both healthy and atypical developmental processes. This is because prior research links the neural correlates of error-related processes to healthy development, risk for anxiety symptoms (Meyer et al., 2018) and exposure to environmental stressors (Mehra et al., 2022). This evidence highlights the importance of enhancing understanding of error monitoring during the transition from childhood to adulthood.

The primary goal of the current study was to use event-related potentials (ERPs) and functional magnetic resonance imaging (fMRI) to map relations between age and the neural generators of error monitoring. We also adopted a secondary goal that considers the specificity of potential relations with the ERN and extends other recent work (Lo, 2018). For this secondary goal, we investigated relations between age and the N2. Most studies investigating the neural correlates of error monitoring utilize a single imaging modality. These studies identify the frontally localized error-related negativity (ERN) ERP component and fMRI activation in the dorsal anterior cingulate cortex (dACC) as error markers. However, other brain areas, such as the posterior cingulate cortex (PCC), are active during error monitoring and also express error-related fMRI activation (Ridderinkhof et al., 2004; Wittfoth et al., 2008). Several findings, mainly from studies with adults, show

that the cingulate cortex is the most likely generator of the ERN activity (Agam et al., 2011; Herrmann et al., 2004; Tamnes et al., 2013). These findings show that multiple areas of the cingulate cortex are involved in error monitoring, with particular reference to the dACC and PCC. Several factors may be the cause of such a difference in the localization of error-related areas, with technique, age, and individual differences playing important roles. Structural brain characteristics also seem to be related to the ERN amplitude. Specifically, white matter properties and myelination of the left posterior cingulate, along with gray matter volume of subareas of the ACC, show significant relations with the ERN response in adults (Araki et al., 2013; Grydeland et al., 2016; Westlye et al., 2009). On the other hand, the relation between cortical thickness and surface area of the cingulate cortex fails to show a relation with the ERN activity in younger subjects (Overbye et al., 2019). It is well documented that across adolescence and into early adulthood there are changes in gray matter (e.g., cortical pruning, decrease in thickness; Norbom et al., 2021), white matter (e.g., increases in myelination particularly in prefrontal areas, Giorgio et al., 2010), and diffusion-based connectivity (e.g., the superior longitudinal fasciculus; Conte et al., 2023). Combining data from multiple modalities with complementary strengths could illuminate specific mechanisms related to the many brain areas, including the dACC and PCC, that support error monitoring.

Neuroimaging studies using fMRI find strong activation in frontal brain areas on tasks requiring relatively high levels of conflict resolution. These areas include the dACC and other cingulo-opercular regions, dorsolateral prefrontal cortex (DLPFC), and other prefrontal regions (Carter et al., 1998; MacDonald et al., 2000; Ridderinkhof et al., 2004; Roe et al., 2021; Taylor et al., 2007; van Veen et al., 2001). The dACC is more active in various tasks requiring performance monitoring and error detection (Le et al., 2021; Nee et al., 2007; Ridderinkhof et al., 2004; Weiss & Luciana, 2022). Performance monitoring and error detection mechanisms have been investigated also through event-related potential measures. The N2 and ERN are ERP components associated with control and error monitoring tasks (Lo, 2018; Yeung et al., 2004). The N2 is considered a neural marker of conflict detection (Eriksen & Eriksen, 1974), where it shows larger amplitude for incongruent relative to congruent flankers (Folstein & Van Petten, 2008). It is usually measured in Fz and Cz, and other frontal-central EEG channels (e.g., FCz, PCz), and includes several sub-components linked to different cognitive mechanisms. Within the N2 group, several cognitive processes are linked to the N2b component, ranging from response inhibition, stimulus conflict, emotional control, and stimulus discrimination, whereas

the N2c is more closely associated with stimulus discrimination and response priming processes (Folstein & Van Petten, 2008).

The ERN relates to performance monitoring, error detection, and error correction (Yeung & Summerfield, 2012). The numerical difference between the ERN on error trials and the negative ERP response following correct responses (i.e., correct responses negativity, CRN) is defined as ΔERN and considered a reliable neurophysiological index of error processing (Clayson, 2020; Meyer et al., 2013). The ERN activity is also associated with individual differences in anxiety (Weinberg et al., 2012) and temperamental factors, such as behavioral inhibition, making the investigation of neural generators of error monitoring important for understanding the risk of developing social anxiety (Buzzell, Troller-Renfree, et al., 2017, Buzzell et al., 2021; Fox et al., 2021).

Age differences in error monitoring skill manifest in the ERN ERP (Buzzell, Richards, et al., 2017; Davies et al., 2004; Gavin et al., 2019; Ladouceur et al., 2007; Lo, 2018; Overbye et al., 2019; Roe et al., 2021; Taylor et al., 2018; for reviews, see Boen et al., 2022; Lo, 2018; Tamnes et al., 2013). Lo (Lo, 2018) reported a meta-analysis of the developmental changes in the ERN and N21 from childhood to adulthood. There were minimal changes in the ERN during childhood, that is, 5–10 years, but significant increases occur during adolescence, with a leveling off in adulthood. A more recent meta-analysis finds a correlation between age and ERN amplitude of −.230 in children from 6.1 to 18.7 years (Boen et al., 2022), indicating an increase in ERN amplitude with increasing age. Of note, Lo (2018) also reported a decrease in N2 amplitude, related to pre-conflict monitoring and the ignoring of distracting information. As children's ability in performance monitoring tasks to attend and ignore distracting information increases with age, so a concomitant decrease occurs in N2 over age (Lo, 2018).

Although the ERN is known to exhibit protracted development across the adolescent window, it remains unclear if and how the neural correlates of the ERN change during this time frame. An improved understanding of these changes could inform neuroscientific models of adolescent anxiety symptom development. This is because the ERN relates to risk for anxiety disorders (Buzzell et al., 2021; Fox et al., 2021; Meyer, 2022; Moser et al., 2013), which tend to emerge across the adolescent window. Extant systems-neuroscience models relating the ERN to anxiety tend to assume age-related stability in the neural basis of the ERN. However, some evidence finds neural regions generating the scalp-level ERN to differ among adolescents and adults (Buzzell, Richards, et al., 2017; Davies et al., 2004). Thus, further work might consider whether the neural basis of the ERN changes with age. This could improve understanding of normative error monitoring development as well as developmental sensitivity for models of anxiety disorder onset. Cortical source reconstruction of ERP signals recorded on the scalp may shed light on the neural generators of error-related responses. Reviews of the cortical sources of the ERN suggest the dACC as the source (Iannaccone et al., 2015; Lo, 2018; Tamnes et al., 2013; van Veen & Carter, 2002b) leading to the idea that the N2 and ERN components share a common neural substrate in the dACC (Botvinick et al., 2004; Lo, 2018; van Veen & Carter, 2002b; van Veen & Carter, 2006). Recent studies have questioned this conclusion. Agam et al. (2011) examined the location of the ERN in EEG and magnetoencephalography (MEG) data, as well as error-related fMRI activations. In that paper, approximately half of the studies cited find a source clearly in the anterior portion of the dACC, similar to fMRI results (Aarts & Pourtois, 2010; Alain et al., 2002; Dehaene et al., 1994; Ladouceur et al., 2007; Mathewson et al., 2005; Segalowitz et al., 2010; van Veen & Carter, 2002a; Vocat et al., 2008). The remaining studies find an ERN source in the very posterior portion of the dACC or in the PCC (Herrmann et al., 2004; Hochman et al., 2009; Munro et al., 2007; O'Connell et al., 2007; Santesso & Segalowitz, 2008; Vlamings et al., 2008; Vocat et al., 2008). Simultaneous EEG and fMRI recordings suggest that at the peak of the ERN activity several cortical areas, including the bilateral PCC, and subcortical brain regions show hemodynamic responses (Donamayor et al., 2012), and more caudal portions of the ACC are activated during later ERN latencies involved in error detection processes (Edwards et al., 2012). Overall, this evidence suggests a central, but not exclusive, role of the ACC in error monitoring.

Two studies clearly show the source of the ERN to lie in the PCC. Agam et al. (2011) was a multimodal study of errors occurring in an antisaccade task using EEG and MEG recorded simultaneously, and fMRI recorded in a separate session. They reported the location of the ERN source, measured with EEG and MEG, in the dorsal region of the PCC bilaterally. fMRI results obtained in a separate session showed that error activations were localized in the dorsal region of the ACC, also bilaterally, with only a sub-threshold activation in the PCC (Agam et al., 2011).

More recently, we performed a source analysis of the ERN in participants from 9 years of age to adulthood in a flanker task, leveraging MRI-informed finite element method (FEM) head models to constrain the source analysis (Buzzell, Richards, et al., 2017). We identified an increase over age in the ERN amplitude, especially at central-parietal electrodes (e.g., CPz). In line with the prior study by Agam et al. (2011), we identified the largest source of ERN within the dorsal region of the PCC. Smaller amplitude source activity was also identified in

several other areas, with accompanying smaller changes over age in ERN source amplitude.

The current multimodal study extends our past work in two ways. First, we extend previous data in one modality (Buzzell, Richards, et al., 2017) to examine age differences in spatial and temporal dynamics of error and performance monitoring from early adolescence to early adulthood. More importantly, we add a much larger sample, including subjects studied longitudinally, and we conduct multimodal analyses comparing brain function from adolescence through adulthood. This period represents a window of vulnerability for the onset of many neurodevelopmental and mental disorders. Current data suggest that behavioral measures are less sensitive indicators than neural measures of developmental processes related to risk (Moser et al., 2013; Tang et al., 2020). Identifying age-related differences in neural circuits involved in error monitoring will deepen our knowledge of typical cognitive neurodevelopment and inform studies of atypical developmental patterns. In particular, the ERN has been identified as a predictor of increased anxiety risk across development (Fox et al., 2022; Meyer, 2017, 2022). The investigation of brain functional responses would improve models of performance monitoring and inform future studies aiming to characterize the relationship between psychopathology and error monitoring systems.

Electrophysiological responses and hemodynamic activity were recorded sequentially while participants performed a flanker task. Distributed source localization obtained using individualized head models from participant's structural MRI allowed us to account for individual anatomical differences in the reconstruction of neural generators of scalp ERP responses. The use of different neuroimaging modalities would help to inform on the activation of a functional cluster of brain areas involved in complex cognitive processes, such as performance and specifically error monitoring, and shed light on the timing in which specific functional responses unfold. Furthermore, by assessing the relation between the EEG source generators and the cluster of fMRI brain activation we would identify commonalities in the responses originating from complimentary techniques. We predicted that the N2 and ERN activity would be modulated by conflict and error processing, respectively. The fMRI activation was predicted to extend to several cortical areas, with only a subset of regions overlapping with the generators of the scalp activity occurring at the time of the main ERP involved in error monitoring mechanisms, that is, the ERN. This multimodal imaging approach examined the extent to which the topographical distribution and timing of neural activity during error monitoring processes may change as a function of age.

2 | METHOD

2.1 | Participants

One hundred fifty-seven participants ranging in age from 9.58 to 43.59 years were enrolled in the study, and one hundred twenty-nine participants provided usable EEG and fMRI data. Preliminary eligibility was based on participant's health condition, IQ > 70, and an MRI-safety screening form. Participants were recruited using two approaches. A total of 51 subjects, described in Buzzell, Richards, et al. (2017), were recruited through the NIMH pool of healthy volunteers. These subjects were recruited by advertisements and by word of mouth. All subjects recruited with the first approach were only studied once. A total of 78 subjects, described in Smith et al. (2020) and Cardinale et al. (2021), were recruited from a longitudinal sample followed since infancy. The participants from this study were included only if they had an EEG, structural MRI, and fMRI sessions at 12 or 15 years of age. Twenty-eight participants from this sample were tested at both 12 and 15 years. Although this sample was enriched to represent a wide range of infant temperament, neither of the two samples included in the present study had any mental health-related inclusion or exclusion criteria. Information about recruitment procedures, participant health, and screening measures may be found in prior publications (Buzzell, Richards, et al., 2017; Cardinale et al., 2021; Smith et al., 2020). All participants over the age of 18 provided written informed consent; for participants under the age of 18, parents signed consent and youth signed assent. The Institutional Review Boards of the University of Maryland (UMD) and the National Institute of Mental Health (NIMH) approved all procedures, which were conducted according to the Declaration of Helsinki. The participants were split into three age groups for the analyses: 12 years, 15 years, and adults. Age-appropriate average MRI templates were used for all groups (see Age-appropriate Average Templates section). Each participant had an EEG and an fMRI session. The age for each group for the EEG session had a range from 9.86 to 13.93 years ($N = 57$, M = 12.69, SD = 0.799, 21 females), 13.83 to 17.47 years ($N = 69$, M = 15.76, SD = 0.775, 31 females), and 17.19 to 43.59 ($N = 31$, M = 26.29, SD = 7.335, 11 females). The age for each group for the fMRI session was 9.58–14.78 (M = 12.76, SD = 0.953), 14.08–17.17 (M = 16.27, SD = 0.941), and 17.17–43.42 (M = 26.28, SD = 7.313). There were 129 participants who completed both the fMRI and the EEG: 12 years ($n = 52$, age M = 12.66, SD = 0.805, 21 females, 2 Asian, 15 Black, 4 Hispanic, 31 Caucasian); 15 years ($n = 51$, age M = 15.71, SD = 0.832, 21 females, 5 Asian, 9 Black, 6 Hispanic, 31

Caucasian); adults ($n = 26$, age M = 7.33, SD = 7.332, 11 females, 8 Asian, 4 Black, 14 Caucasian).

2.2 | Procedure

The participants performed a modified flanker task at UMD while EEG data were recorded, and the same task at NIMH where functional MRI was recorded. The order of EEG and fMRI tasks was counterbalanced and randomly determined so that the mean age at testing for the three age groups was approximately equal for the EEG and fMRI sessions. Trial structure was identical in the EEG and fMRI tasks, but inter-trial intervals and trial numbers were tailored to the imaging modality (see next section). Structural MRIs were collected for the purpose of creating head models for current source reconstruction and providing a common spatial reference for EEG and fMRI analyses.

2.3 | Experimental task, apparatus, and stimuli

Participants completed a modified flanker task (Eriksen & Eriksen, 1974) in an EEG session and separately in a fMRI session. The flanker task used a central arrow flanked on the side with arrows pointing the same (congruent trial) or opposite (incongruent trial) direction and participants indicated the direction of the central arrow with a button press (Figure S1). The stimuli were shown in white against a dark gray background. Prior to completing the experimental task, participants performed 16 practice trials, followed by feedback to maintain accuracy at a level that would ensure an adequate number of errors occurred, consistent with the recommendations by Gehring and colleagues (Gehring et al., 2012). The EEG session consisted of 10 blocks of 32 trials ($N = 320$). The fMRI session consisted of four six-minute runs. Each run consisted of 108 trials ($N = 432$). All four runs were completed by 139 participants, and three runs were completed by 2 participants. In the fMRI version, trials consisted of a 300–600-ms fixation cross, a 200-ms flanker stimulus, and then a 1700-ms blank screen. Additional details of the EEG session can be found in Buzzell, Richards, et al. (2017) and of the fMRI session in Smith et al. (Smith et al., 2020) and Cardinale et al. (2021). Participants were included in the analyses if they made a minimum of 10 errors on incongruent trials during each of the EEG and fMRI sessions. The average number of good trials after signal processing for the EEG was 312 (SD = 75.26), and for the fMRI was 421 (SD = 26.8). Four subjects had less than 10 incongruent-error EEG trials and were excluded from the analysis, leaving 153

participants with usable EEG (12 years: M = 130 congruent trials; M = 116 incongruent trials; M = 108 correct trials; M = 33 error trials. 15 years: M = 165 congruent trials; M = 154 incongruent trials; M = 130 correct trials; M = 39 error trials. Adults: M = 180 congruent trials; M = 171 incongruent trials; M = 152 correct trials; M = 40 error trials).

There were 558 fMRI runs, and only 15 runs had less than 10 incongruent-error trials. There were 16 subjects who did not pass the fMRI quality control prescreening, leaving 141 participants with usable fMRI. A total of 129 subjects had both EEG and fMRI usable data and were included in the final analyses.

2.4 | EEG acquisition and preprocessing

EEG was acquired using a 128-channel HydroCel Geodesic Sensor Net and EGI software (Electrical Geodesic, Inc.); EEG analysis was performed using the EEGLAB toolbox (Delorme & Makeig, 2004), ERPLAB (Lopez-Calderon & Luck, 2014), and custom MATLAB scripts (The MathWorks) (cf. Buzzell, Richards, et al., 2017). The 128 channels were sampled at 250 Hz with electrode impedance maintained below 50 kΩ. All EEG data were pre-processed with the Maryland Analysis of Developmental EEG (MADE) pipeline (Debnath et al., 2020) (v1.0). The MADE pipeline is implemented in MATLAB (The MathWorks) and uses the toolbox EEGLAB (Delorme & Makeig, 2004) and its plugins "firfilt", FASTER (Nolan et al., 2010), ADJUST (Mognon et al., 2011), and Adjusted-ADJUST (Leach et al., 2020). All default options of the MADE pipeline were used (Debnath et al., 2020). Offline, data were re-referenced to an average reference and filtered with a Hamming windowed digital FIR filter. Data were high pass filtered at 0.3 Hz with a half-amplitude (−6 dB) cutoff frequency of 0.15 Hz. Data were low pass filtered at 50 Hz with a half-amplitude cutoff frequency of 55 Hz. FASTER was used to identify globally bad channels (Nolan et al., 2010). Additionally, channels were marked bad at the epoch level if voltage exceeded ±125 μV, and any epochs in which more than 10% of non-ocular channels exceeded this threshold were marked bad; otherwise, bad channels were interpolated via a spherical-spline interpolation. Ocular artifact detection and removal was performed with ICA (see Debnath et al., 2020 for detailed ICA steps) paired with Adjusted-ADJUST (Leach et al., 2020), an automated algorithm for identifying artifactual ICA components. The data used in the current study were segmented from −100 through 500 ms relative to stimulus onset for the stimulus-locked ERPs and −100 through 500 ms relative to response onset for the response-locked ERPs. The EEG segments were assigned to congruent trials, incongruent trials, incongruent-correct trials, and incongruent-error trials. The stimulus- and response-locked ERPs were corrected using

the 50 ms preceding the locked onset time. This window allowed us to perform a baseline correction without including peaks from previous ERP components.

The three-dimensional coordinates of 14 anatomical and electrode fiducial landmarks were digitized using the Polhemus Fastrak during the EEG session. The positions of the electrodes on the T1-weighted MRI were computed by co-registering the digitized scalp fiducial and digitized electrode fiducial locations from the EEG session with corresponding positions on the structural MRI. The HGSN 128 positions were estimated by using the scalp fiducial locations, the electrode fiducial locations, and the electrode locations from the age-appropriate average template. The 10–10 positions were computed on the structural MRI head (Jurcak et al., 2007; Richards et al., 2015).

2.5 | MRI acquisition

A T1-weighted and T2-weighted structural MRI images were acquired in a 3-Tesla MR750 GE scanner with a 32-channel head coil. The T1-weighted scan was a magnetization-prepared rapid acquisition gradient-echo sequence (MPRAGE; sagittal acquisition; TI/TE = 425/min; flip angle = 7°; FOV = 25.6; Matrix 256 × 256; Slice thickness = 1 mm; bandwidth = 25 Hz). The T2-weighted scan was a fast relaxation fast spin-echo sequence was acquired (FRFSE-XL; sagittal acquisition; TR/TE 15000/80 ms; FOV = 25.6; Matrix 256 × 256; Slice thickness = 1 mm; bandwidth = 31.25 Hz). The DICOMM files were compiled into NIFTI-GZ files. The T1-weighted MRI volume was registered to the age-appropriate average template using FSL's flirt (Jenkinson et al., 2002; Jenkinson & Smith, 2001).

The functional MRI images were obtained during performance of the flanker task in a 3T GE Scanner using a 32-channel head coil. Each functional imaging run consisted of 170 whole-brain (forty-two 3-mm axial slices of 2.5 × 2.5 mm resolution) T2-weighted echoplanar images (TR = 2000 ms, TE = 25, flip angle = 60 deg, 24 field of view, 96 × 96 matrix). The MRI volumes were registered to the T2-weighted volume by placing the images from the four runs into a single 4D volume, using FSL's MCFLIRT (Jenkinson et al., 2002) to do motion correction, obtaining the mean BOLD volume from the motion corrected images, and using FSL flirt (Jenkinson et al., 2002; Jenkinson & Smith, 2001) to register to the T2-weighted MRI volume.

2.6 | Age-appropriate average templates

Separate average templates were used for the three testing ages. Age-appropriate average templates were selected from the Neurodevelopmental MRI Database (Richards

& Xie, 2015; Richards et al., 2016). The templates for the 12- and 15-year-old groups were average templates for 12- and 15-year-olds, and the average template for adults was the 20–24 years template. The templates were used in the electrode co-registration procedure, to display 3D results of source data, for fMRI display and analysis, and for relating MNI templates to ages and individuals. Each participant's structural MRI was registered with FSL's flirt (Jenkinson et al., 2002; Jenkinson & Smith, 2001) to the age-appropriate average template. The flirt affine registration matrix was used to translate between participant space and average template space, and through average template space from participant to the MNI space.

2.7 | ERP and source analysis

The EEG data were analyzed as event-related potentials (ERP), and cortical source analysis was used to identify the cortical generators of the ERP. For the goal of the current study, we reported analyses and results of the N2 and ERN ERPs. Additional stimulus-locked (i.e., P1, N1, P2) and response-locked (i.e., Pe) components were investigated for completeness and reported in the Supplementary Information. Details of each ERP component are listed in Table 1 and include the time-window, polarity, and channels of interest utilized to define each ERP. Response-related activity for the incongruent correct trials was subtracted from the ERN on the incongruent error trials (ΔERN).

Cortical source analysis was used to identify the cortical generators of the ERP components. This analysis requires several processing steps, recently outlined in Conte and Richards (2022); also see detailed description for this study in Buzzell, Richards, et al. (2017) and Gao et al. (2019), and general information on source analysis (Michel et al., 2004; Vorwerk et al., 2014). The steps included: (1) segmenting the head using the T1-weighted and T2-weighted into component media with varying conductivity values, including skin 0.35 S/m, skull 0.0132 S/m, CSF 1.79 S/m, WM 0.2 S/m, GM 0.33 S/m, dura 0.33 S/m, muscles 0.35 S/m, eyes 0.5 S/m, and nasal cavity 0.0048 S/m. Of note, segmentation procedures were performed using FSL tools for all media, except for eyes and nasal cavity, which were manually segmented. (2) computing a volume conduction model (i.e., head model) describing how electrical current flows through the head, using the Fieldtrip computer program (Oostenveld et al., 2011; Vorwerk et al., 2019; Vorwerk et al., 2013) and Iso2Mesh (Fang & Boas, 2009; Tran et al., 2020) programs, represented as a tetrahedral mesh with conductivities for each tetrahedron; (3) creating a source model consisting of the segmented GM and eyes with a tetrahedral mesh

TABLE 1 Event-related-potential (ERP) components. The EGI 128-channel electrodes ERP were translated into 10–10 locations using a spherical-spline transformation.

Name	Timing	Direction	10–10 electrodes
Stimulus-locked ERPs			
P1	75–170	Positive	POz, Oz, Iz, PO7, PO8, O1, O2, I1, I2
N1	P1 latency to 250	Negative	POz, Oz, Iz, PO7, PO8, O1, O2, I1, I2
N2	N1 latency to 300	Negative	AFz, Fz, FCz, F1, F2
P3	N2 Latency to 500	Positive	Cz, CPz, Pz, POz
Response-locked ERPs			
ERN	0–100	Negative	AFz, Fz, FCz, Cz, CPz
Pe	200–400	Positive	AFz, Fz, FCz, Cz, CPz

(Fang & Boas, 2009; Tran et al., 2020); (4) identifying the positions of the electrodes on the T1-weighted MRI by co-registering the digitized fiducial and electrode locations from the EEG session with corresponding positions on the scalp MRI; (5) computing the lead-field matrix with Fieldtrip (Oostenveld et al., 2011; Vorwerk et al., 2013; Vorwerk et al., 2019), which consists of a matrix relating the 128 electrode leads to the voxel locations in the source model for current generation from the leads through the head model media conductivities to the source model voxel locations; (6) computing the inverse spatial filter created with the exact low-resolution electromagnetic tomography (eLORETA) method (Pascual-Marqui et al., 2011; Pascual-Marqui et al., 2006) for each subject that may be multiplied with the selected ERP data to reconstruct the current density in the cortex that generates the EEG scalp potential recorded in the EEG session (i.e., current density reconstructed (CDR) values). A hallmark of this procedure is the emphasis on a realistic model of current generation using individualized head and source models for each participant, finite element method (FEM) approach to the forward solution, distributed source model approach to generate a distribution of the CDR across the cortex.

The result of the current source reconstruction is a sample-by-sample estimate of the CDR for each voxel in the source model in an ERPLab format, for each experimental condition (congruent, incongruent, incongruent-correct, incongruent-error) (Conte & Richards, 2022). These data can be further combined by calculating the mean level for each sample and condition over ROIs (see below). A dependent variable for the analysis acquired by taking the peak latency of the relevant ERP component, using a quadratic polynomial filter to convolve the CDR with a peaked ERP component, and taking the resulting value as the variable for analysis. When displaying the sources of the ERN, the source analysis of the incongruent correct and incongruent error trials was computed

separately at the latency of the ΔERN component, and the display is from the error minus correct incongruent sources (ΔCDR). When displaying the sources of the N2, the source analysis of the correct congruent and correct incongruent trials was computed separately at the latency of the N2 component and displayed as the sum of the sources from the two trial types. Typically for the N2, the responses in the high-conflict condition are subtracted from the low-conflict condition. However, in our data, the ERP difference was small (~0.4 μV), and thus, the resulting source differences were also small (<0.4 μA/mm³). Thus, we chose to sum the congruent and incongruent N2 to illustrate the location of the N2. See Supplemental Information and Discussion for further information.

The sample-by-sample ΔCDR values also can be translated from the ERPLab format into 3D MRI volumes. The quadratic dependent variable can be assigned to each voxel in a 3D MRI volume. The 3D files from individuals were combined into a single 3D volume by using the T1-weighted to age-appropriate template registration. The ΔCDR was analyzed as a function of ROIs derived from an analysis of "error" studies from the Neurosynth (Yarkoni et al., 2011) meta-analysis.

2.8 | Neurosynth ROIs

ROIs were defined based on the Neurosynth (Yarkoni et al., 2011) meta-analysis www site (https://neurosynth.org/). The Neurosynth site was used with "error" as a search term to construct an MRI volume with error > correct contrasts. The three largest clusters using the FSL cluster tool in this MRI volume were in the dACC, left insula, and right insula. We also relaxed the search with a *T* value of 5 and the *minextent* value set to 70 and found three additional clusters: PCC, left superior parietal lobe, and right parietal lobe. Figure 1 shows the ROIs found from the cluster analysis of the Neurosynth meta-analysis

Neurosynth ROIs

- Dorsal Anterior Cingulate
- Right Insula
- Left Insula
- Posterior Cingulate
- Right Superior Parietal Lobe
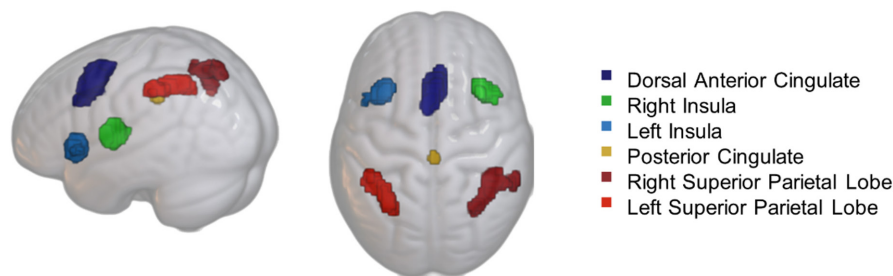- Left Superior Parietal Lobe

FIGURE 1 Neurosynth ROIs overlaid on the rendered adult brain template.

for the error contrast on the 20–24 years template. The MNI brain was registered to each average template brain (12, 15, and 20–24 years), and the six Neurosynth ROIs were translated into the average template space. The Neurosynth ROIs from the average template space were translated into each individual T1-space.

2.9 | fMRI analysis and fMRI-Constrained ROIs

The BOLD responses in the fMRI were analyzed using a similar approach detailed in Gao et al. (2019). The fMRI preprocessing was carried out using FSL (FMRIB software library, version 5.0, www.fmrib.ox.ac.uk.fsl) and SPM 12 (http://www.fil.ion.ucl.ac.uk/spm) and was designed by Hanayik and Richards (2018). The procedure included head motion detection with FSL's MCFLIRT, spatial smoothing with FSL's fslmaths, a general linear model (GLM) using SPM12 with an event-related design, with a temporal derivative for the HRF, with the regressors including the point-onset for each trial (0 ms duration) classified as congruent-correct, incongruent correct, and incongruent error. We did not include congruent error trials because the number of congruent error trials was too small for many subjects, and we had no contrast hypothesis for congruent-error trials. The BOLD fMRI activities for the four runs of each participant were separately preprocessed. The incongruent-error greater than incongruent-correct contrast values for each participant and run were concatenated into a single 4D MRI volume and evaluated as a one-way analysis in PALM (Winkler et al., 2014). The BOLD fMRI volumes, concatenated and summed, were registered to the T2-weighted MRI volumes with FSL flirt to compare the fMRI results in the same space as the CDR results.

The fMRI results were used to condition the CDR analyses. For each participant, the incongruent-error greater-than-correct contrast from the four runs was translated in the participant T1 space (3 mm voxels, no interpolation) and averaged across the four runs. The source analysis results for each participant resulted ΔCDR values for each tetrahedron of the source model.

To condition the CDR results, any voxel from the fMRI analysis that overlapped with a tetrahedron element for ΔCDR was multiplied by the value of the ΔCDR for that tetrahedron. Note that all tetrahedral elements do not intersect with the fMRI voxels due to the resolution differences between the fMRI and the source models, and not all fMRI voxels intersected with a tetrahedral element due to the whole brain fMRI representation and the source model elements. The value from this analysis is the "fMRI-conditioned ΔCDR."

2.10 | Analysis strategy

The analysis of the data was done first on the individual modalities (ERP, CDR, fMRI), and then, on the relation between the CDR and fMRI. The ERPs were analyzed as a function of electrode position and age for the stimulus-locked and response-locked ERPs. The ΔCDR was analyzed as a function of Neurosynth ROIs and age for the response-locked ERPs, emphasizing the error detection ERPs. The multi-modal relation between the ΔCDR and fMRIs was examined with the fMRI_ΔCDR as a function of the Neurosynth ROIs and age. The analyses were done with Proc GLM and Proc Mixed of SAS (version 9.4) software (SAS Institute Inc., Cary, NC). The repeated measures were analyzed with the Proc GLM, with the repeated command for repeated electrode or ROI factors, to compute an approximated Huynh-Feldt correction (Huynh, 1978; Huynh & Feldt, 1980; Lecoutre, 1991). Twenty-eight of the 15-year-olds were also tested at 12 years, creating unbalanced designs with respect to the participants. Proc Mixed was used to estimate the effects of the factors, using fixed effects for trial type and age, fixed effects for electrodes, and random effects for participants and nested (repeated) factors, with REML estimation. The Proc Mixed results for repeated factors were reported only for those that met the appropriate level of significance with the Huynh-Feldt correction. Post hoc or planned comparisons were performed with the Scheffé's error-protection strategy. The results replicating prior studies are summarized in the Results section, with details in the Supplemental Information.

The original data are available on NDAR. The code for the pipeline and analyses are available on NITRC.org.

3 | RESULTS

3.1 | Stimulus-locked and response-locked ERPs

We reported here analyses and results of the N2 and ERN components, whereas results of other ERPs (i.e., P1, N1, and Pe) are reported in Supplementary Information for completeness. The N2 stimulus-locked ERP was analyzed in relation to the congruent and incongruent conditions for the three testing ages (12 years, 15 years, adults). The peak of the N2 ERP component was analyzed for the frontal-central 10–10 channels (AFz, Fz, FCz, Cz, and CPz) with Age X Trial Type X Electrodes mixed models analysis. There was a significant effect of trial type, $F(1, 150) = 7.01$, $p = .0090$, with only a small difference between congruent (M = −1.73) and incongruent (M = −2.10) trials, but no significant difference for age. There was a significant main effect of electrodes, but no significant interactions involving trial type, age, and electrodes.

Figure 2 shows the ERP for the congruent-correct, incongruent-correct, and incongruent-error trials for the FCz electrode separately for the three ages. The ERN occurred after the peak of the N2 and appears to delay the onset of the P3 on the error trials. The Pe occurred during the P3 on the error trials after the peak of the P3 on the correct trials. Figure S4 shows results for all the midline channels.

The response-locked ERP was analyzed for incongruent-correct and incongruent-error trials. The peak of the ERN was analyzed for the medial frontal-central 10–10 electrodes (AFz, Fz, FCz, Cz, CPz) and age using the difference score between the incongruent-correct and incongruent error trials, with an Age X Electrodes mixed model. There were significant effects of age, $F(2, 130) = 3.43$, $p = .03564$, electrodes, $F(4, 484) = 20.22$, $p < .0001$, and a significant interaction of age and electrodes, $F(8, 130) = 5.19$, $p < .0001$. The electrodes main effect reflects overall levels of the ERN across electrodes. The age-by-electrode interaction reflects differing age effects over the electrodes. The age effect was not significant for the most anterior electrodes (AFz, Fz, FCz), but this effect was significant for Cz (12 years < 15 years = 20 years) and the CPz (12 years < 15 years < 20 years) electrodes. Figure 3a shows
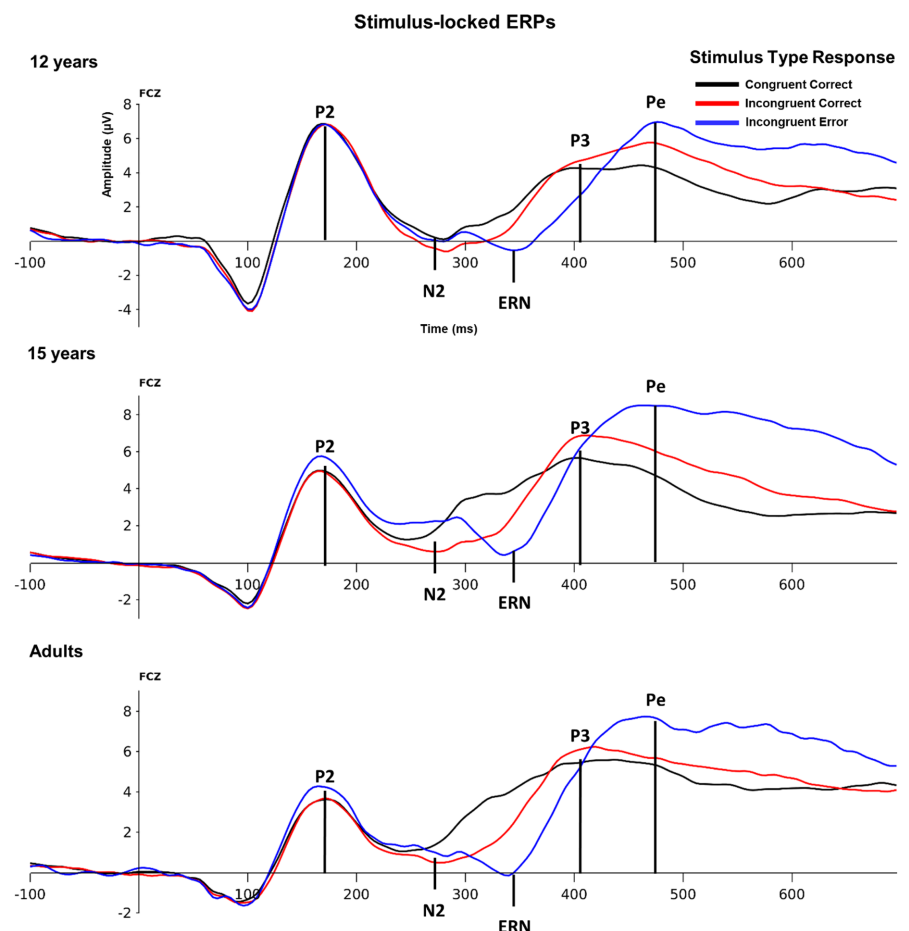

FIGURE 2 Stimulus-locked ERPs for the congruent correct (dotted lines), incongruent error (solid lines), and incongruent correct (dashed lines) conditions on FCz, separately for the three testing ages.
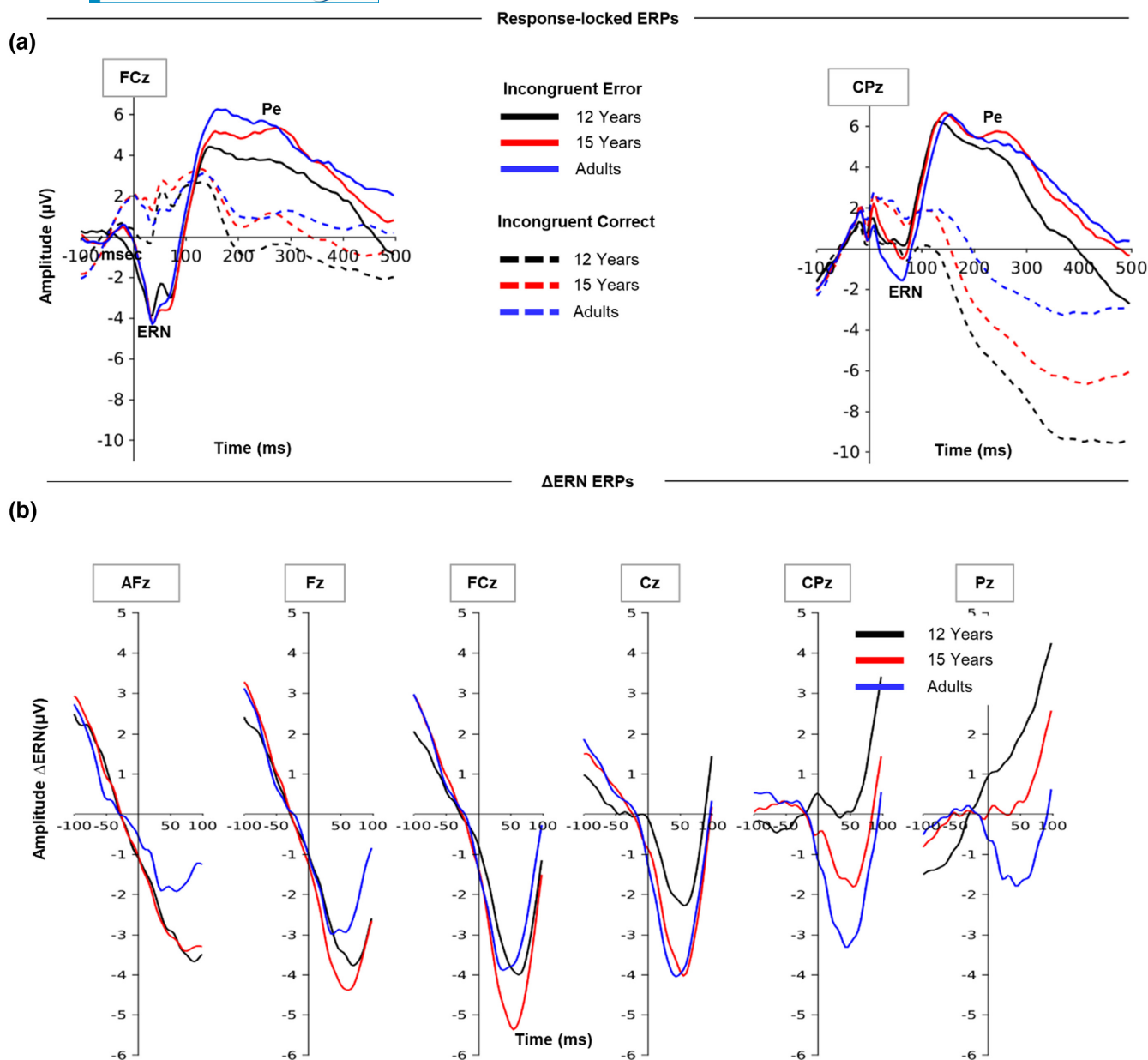
PSYCHOPHYSIOLOGY SPR

FIGURE 3 (a) Response-locked ERPs for the congruent correct and incorrect conditions over fronto- and parietal-central channels. (b) algebraic difference of the ERN activity between error and correct trials (i.e., ΔERN) over five midline channels from frontal to parietal areas. In all panels the black lines represent the activity of 12-year-old participants, the red lines are for the 15-year-old group, and the blue lines are for adult participants.

the response-locked ERPs for the incongruent-correct and incongruent-error trials, separately for the three ages, for two electrodes showing significant differences in correct and error trials. The small negative component near the beginning of the epoch for the error trials, and the divergent positive–negative slow wave for the correct and error trials, is visible in these ERP plots. Figure 3b shows the difference ERP (ΔERN) for the medial channels from AFz to Pz for the first 100 ms following the response, and Figure 4 shows topographical scalp potential maps for the peak of the ΔERN for the three age groups.

Age differences occurred in the spatial distribution of the ΔERN (Figure 4 bottom). The response was largest in the prefrontal channels for the 12-year-olds (e.g., Fz, FCz, Cz) and peaked at FCz. The ΔERN for the 15-year-olds extended to the posterior CPz electrode, whereas the adult ΔERN extended through the Pz electrode. The shift from anterior to mid-posterior electrodes can be seen in the topographical scalp potential maps and the bar graph of the three ages for the midline electrodes (Figure 4). There was a significant age effect for the Cz (12 < 15 = adults) and the CPz (12 < 15 < adults) electrodes, and the age
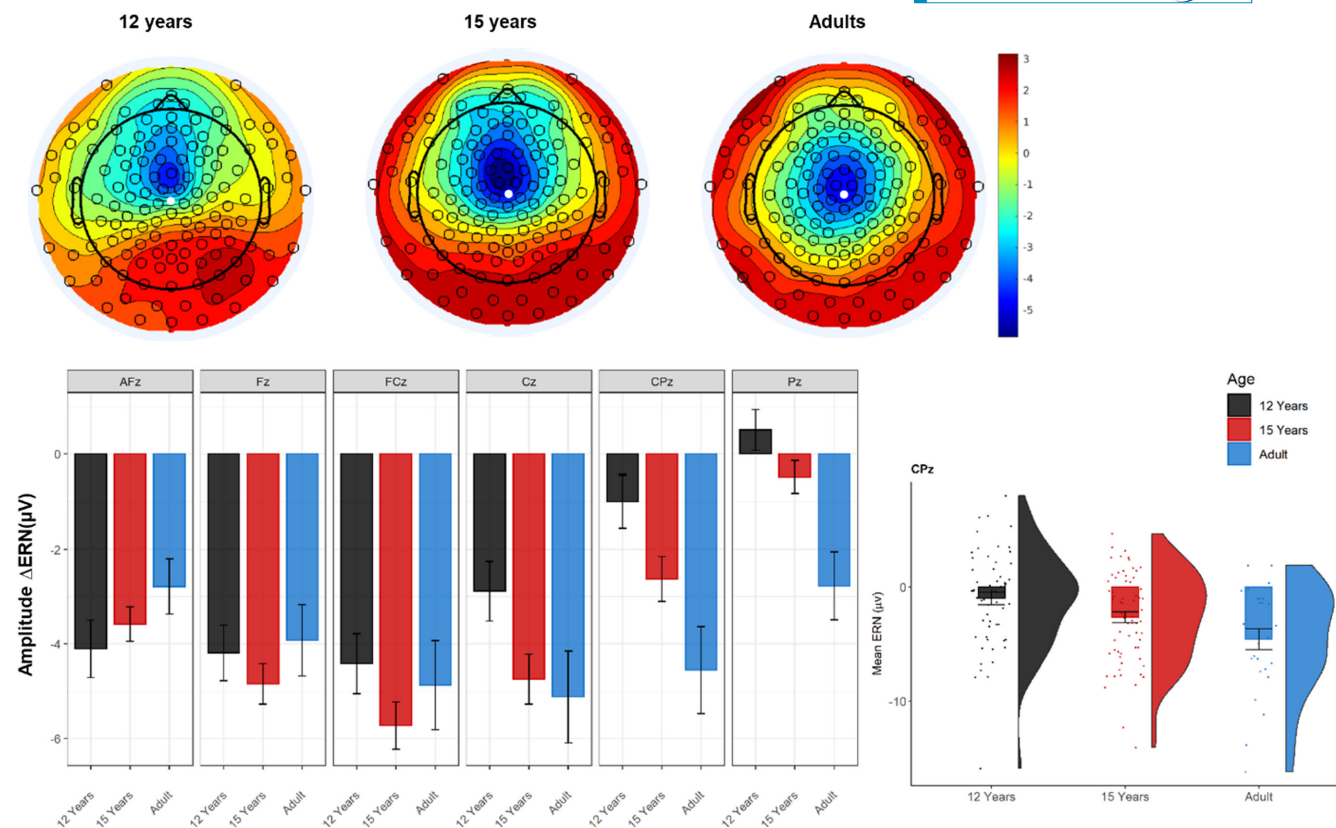
FIGURE 4 Top panels depict the scalp activity at the ΔERN peak for the three age groups. A white circle is placed to mark the location of the reference channels (Cz) to show how the negative central activity moves posteriorly in adult participants versus adolescents. Mean activity around the ERN peak is depicted in the bar graphs as a function of participant age for the midline channels. A raincloud plot is reported for the CPz channel. Full dots represent individual data points. Error bars represent the standard error from the mean.

effect was nonsignificant for the rest of the electrodes (see Supplemental Information).

3.2 | Current source analysis

The current density reconstruction (CDR) was analyzed as a function of Neurosynth ROIs and age for the ΔERN response-locked ERP, emphasizing the error monitoring ERPs. Source analysis was performed on all the quantified ERP components, the results of which are reported in Figure 5. There was a shift of the predominant activity from the posterior to the anterior cortical regions corresponding to the latency of each component. The source of the stimulus locked N2 was in the dACC for all three testing ages. In contrast, the source activity, ΔCDR, at the response-locked ΔERN latency moved from dACC area at 12 years, to the middle cingulate area at 15 years, and to the PCC and superior parietal lobe for the adults. This age-related, anterior-to-posterior change in ΔCDR, within source space, mirrors the observed changes in the scalp-level change in ΔERN topography across age.

The ΔCDR values surrounding the peak latency of the ΔERN component were analyzed in relation to age and the Neurosynth ROIs. The dependent variable for this analysis was the ΔCDR data transformed by a quadratic function centered at the peak latency of the ΔERN. An Age X Neurosynth ROI (dACC, left insula, right insula, PCC, left superior parietal lobe, right superior parietal lobe) mixed model was tested. There were significant main effects of age, $F(2, 120) = 6.38$, $p = .0023$ and ROI, $F(5, 618) = 12.09$, $p < .0001$, but the interaction was not significant. Figure 6 shows the ΔCDR values as a function of time for −100 through 100 ms around the response onset, for the Neurosynth ROIs, along with the average activity at the ΔERN peak. The dorsal anterior cingulate showed a peak at the ΔERN latency, with larger CDR values for the youngest two ages than the adults. The posterior cingulate, and to a lesser extent the superior parietal lobe, showed the adults with a larger ΔCDR than the two youngest ages. Though the interaction of age and ROI was not significant, Scheffé's post hoc tests showed significant age effects for the PCC and right superior parietal ROIs (p's < .05).

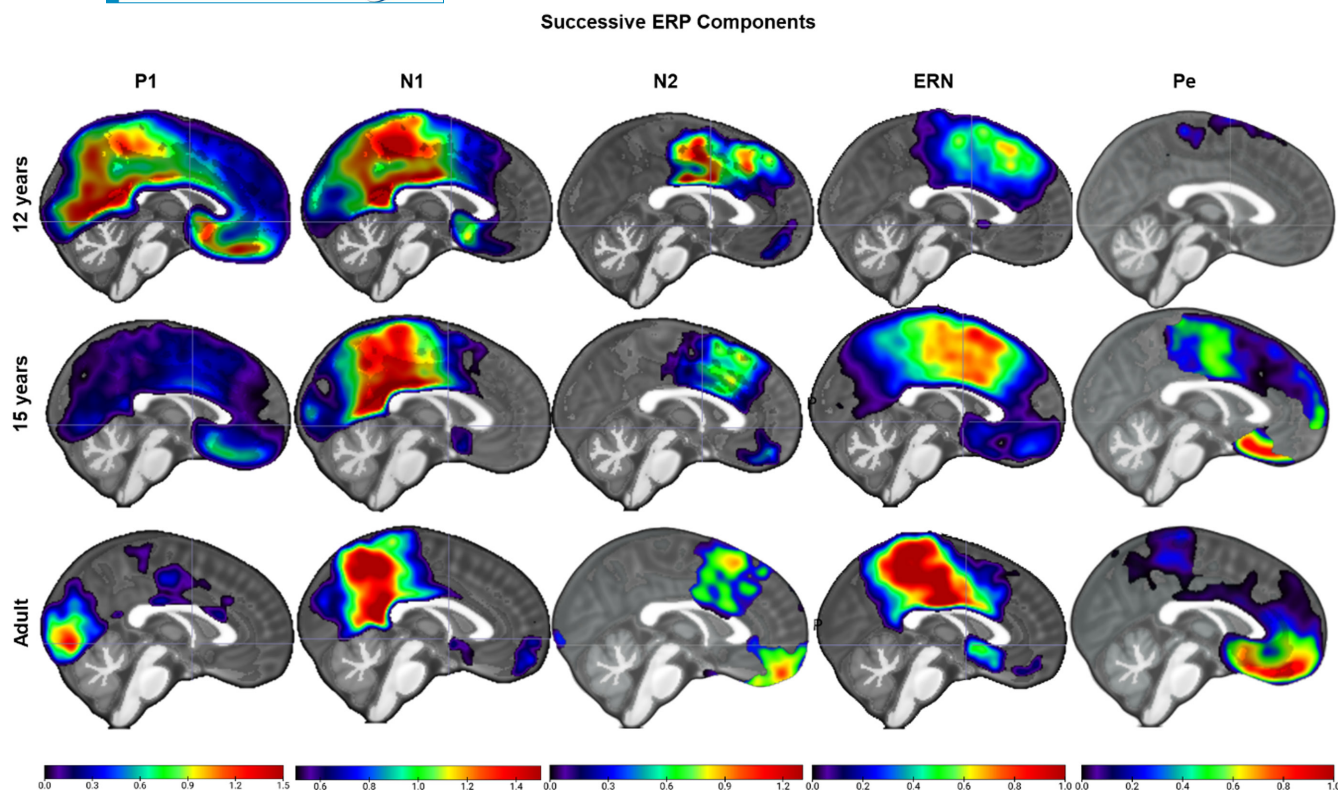CONTE ET AL.

Successive ERP Components

FIGURE 5 Sagittal view of the CDR source activity for each ERP component plotted on the age-specific templates. Note that P1, N1, and N2 are stimulus-locked activities, whereas ERN and Pe are response-locked activities.

3.3 | fMRI BOLD analysis

Figure 7 shows the medial slice of the *T*-values from the PALM permutation effects that were significantly different from 0, and the Gauss-gamma (Gorgolewski et al., 2012) median for that FWEP. There was a large area of activity in the dACC for all three ages, and a smaller area of significant activity near the PCC. Figure 7 also shows a coronal slice near the center of the dACC. The BOLD activity in the right and left insula was significant for the two oldest groups, and the right insula for the 12 years. Not shown in these figures is the significant activity in the superior parietal lobe.

Table 2 shows a cluster analysis for the 15-year-old group. Significant activity in the fMRI showed similar clusters as was found in the Neurosynth ROIs. The 15-year-old group additionally displayed left and right dorsolateral prefrontal cortex, and cerebellum activations. The BOLD fMRI in the 12-year-old and adult groups also showed significant activity in clusters that were similar to those found in the Neurosynth ROIs. The Gauss-gamma adaptive threshold method for voxel-wise error control (Gorgolewski et al., 2012) was used to identify the minimum threshold of the gamma portion of the distribution. This threshold was used for the functional FWEP (family-wise error *p*-value) to localize the ROIs from the fMRI. The

six ROIs from the Neurosynth analysis also were found in the fMRI clusters (Table 2, '*').

3.4 | fMRI-conditioned ERN source activity

The relation between the ΔCDR and fMRI activation was analyzed. Figure 8 shows the 3D rendering of the ΔCDR for the three testing ages and the corresponding fMRI *T* values from the PALM analysis. The predominant activity is evident in the dACC area for the N2 source at all ages, as is the corresponding fMRI BOLD response in this area. The ΔCDR activity occurred in the same location as the fMRI BOLD response for the youngest ages. However, the ΔCDR was located in progressively more posterior locations for the two older ages. Figure S6 shows the ΔCDR on 3D rendered plots for the adults for each of the ERP components ordered by the latency of the component (see Figure 5 for all ages). There was a shift of the predominant activity from the posterior to the anterior cortical regions corresponding to the latency of each component and these regions corresponded to the BOLD fMRI clusters. The shift of the ERN source occurred from the anterior to the posterior areas across the three ages groups and is evident relative to the stability of the position of the N2 source.
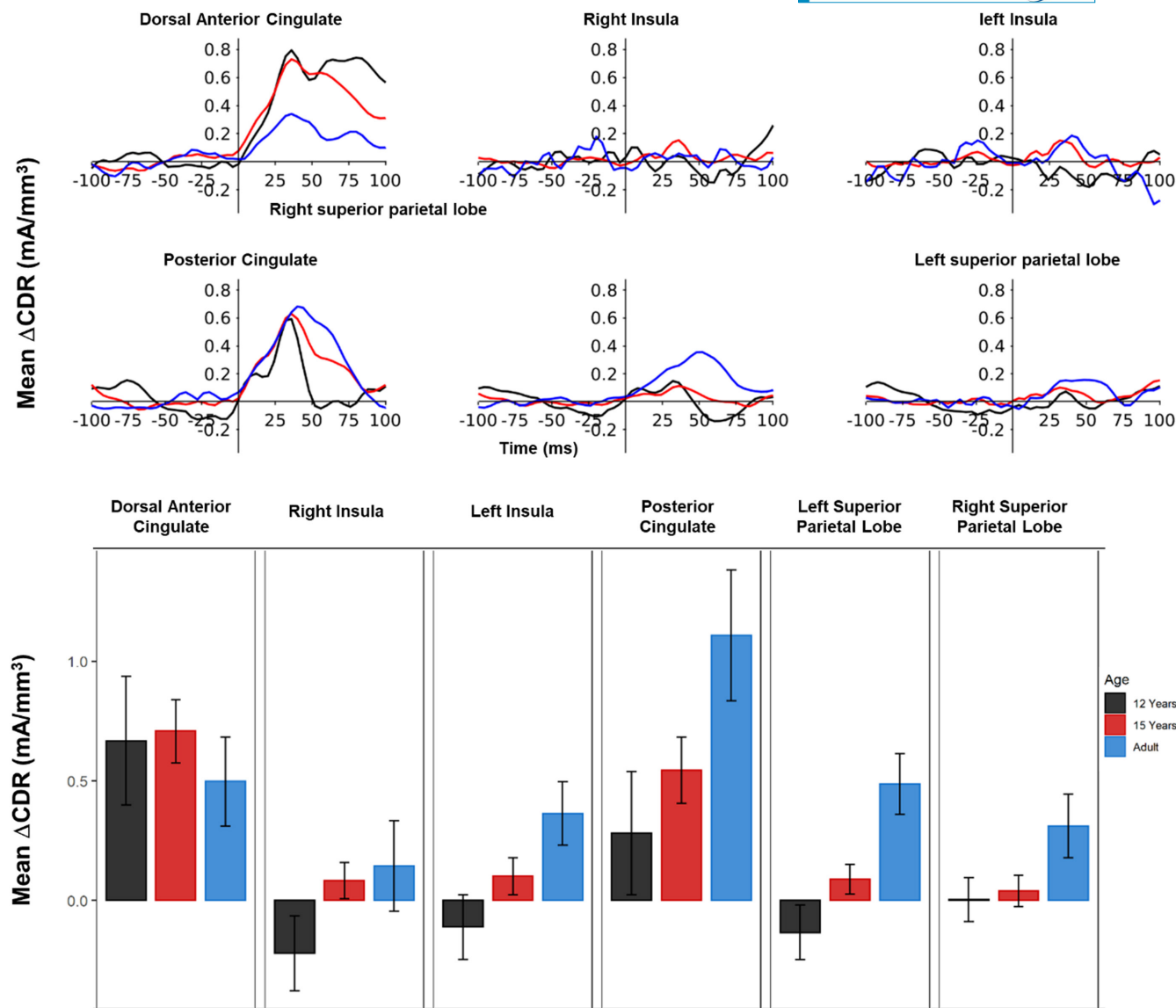
FIGURE 6 The pattern of ΔCDR activity at the latency of the ΔERN component is depicted in the line plots for each considered ROI as a function of participant's age. Bar plots report the average ΔCDR at the peak of the ERN activity. The largest ΔCDR activity was localized in the dACC for the adolescent groups and more posteriorly (PCC) in adults. Raincloud plots depict the ΔCDR activity in PCC as a function of age. Dots represent individual data points. Error bars indicate the SE from the mean.

The fMRI-conditioned ΔCDR values surrounding the peak latency of the ΔERN component were analyzed in relation to age and the Neurosynth ROIs. The dependent variable for this analysis was the fMRI conditioned ΔCDR data transformed by a quadratic function centered at the peak latency of the ΔERN. An Age X Neurosynth ROI (dACC, left insula, right insula, PCC, left superior parietal lobe, right superior parietal lobe) mixed model was tested. There were significant main effects of age, $F_{(2, 96)} = 10.46$, $p < .0001$, and ROI, $F_{(5, 594)} = 9.68$, $p < .0001$, but the interaction was not significant ($p = .0701$). Figure 9 shows the fMRI-conditioned ΔCDR values as a function of time for −100 through 100 ms around the response onset, for the Neurosynth ROIs, along with the average

activity at the ΔERN peak. The bottom panels show bar graphs of the means at the ΔERN latency for these data. The dorsal anterior cingulate showed a peak at the ΔERN latency, with larger ΔCDR values for the youngest two ages than the adults. The posterior cingulate, and to a lesser extent the superior parietal lobe, showed the adults with a larger fMRI-conditioned ΔCDR values than the two youngest ages. Though the interaction of age and ROI was not significant, Scheffé's post hoc tests showed significant age effects for the PCC and right superior parietal ROIs (p's < .05).

Figure 10 shows the CDR values separately for the two ROIs that showed an age effect on the ΔCDR and the fMRI-conditioned ΔCDR, along with the dACC results
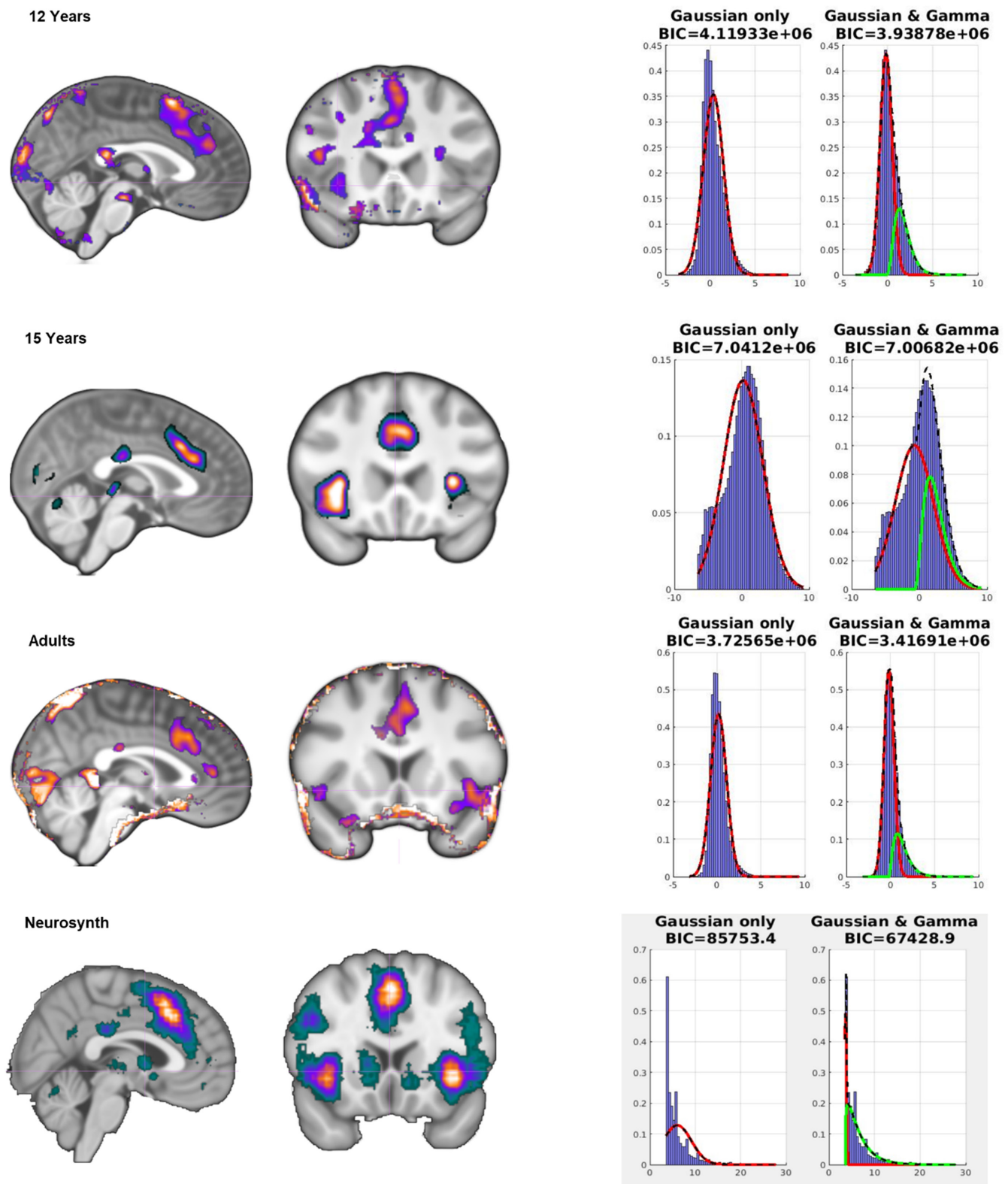
FIGURE 7 *T*-values of the PALM clustering procedure along with the Gamma and Gaussian-Gamma distributions plotted separately for the three testing ages and the Neurosynth data.

TABLE 2 BOLD fMRI ROIs for 15-year-old group.

#	nv	T	MaxS	MaxC	MaxA	CogS	CogC	CogA	Anatomical ROI
9	7373	9	60	135	65	64	123	83.6	Dorsal anterior cingulate*
8	6308	8	23	117	41	27.8	115	54.7	Right insula*
7	4812	7	11	60	84	23.7	60.4	97	Right superior parietal lobe*
6	4121	6	30	143	64	36.9	142	74	Right dorsolateral prefrontal
5	3991	5	106	113	42	99.4	115	55.7	Left insula*
4	1646	4	89	141	64	94.6	141	73.4	Left dorsolateral prefrontal
3	1472	3	62	75	76	63.3	80.4	81.7	Posterior cingulate*
2	1382	2	98	45	21	98.5	44	30	Left cerebellum
1	1183	1	115	61	90	105	59.6	97.5	Left superior parietal lobe*

Abbreviations: #, arbitrary label number; Anatomical ROI, anatomical region for the ROI; CogS, CogC, CogA, center of gravity saggital, coronal, and axial locations; MaxS, MaxC, MaxA, maximum saggital, coronal, and axial locations, respectively; nv—, number of voxels; T–, T value.

*Areas selected from the Neurosynth atlas.

(from Figures 6 and 9). There were similar patterns between the ages for the dACC and superior parietal ROIs for the two types of data. The age effect in the fMRI-conditioned ΔCDR for the PCC ROI was more obvious, showing both the decreased temporal range of the values for the 12-year-olds, and an attenuated amplitude.

4 | DISCUSSION

The current study examined age differences in performance monitoring and error detection. The ERN amplitude increased and shifted from anterior frontal electrodes to central-parietal electrodes, with the cortical generators localized in the dorsal portion of the anterior cingulate gyrus (dACC) for the 12-year-old group and the posterior portion of the cingulate gyrus (PCC) in the 15-year-old group and adults. Conversely, the source of the N2 ERP component was located in the dACC at all testing ages. The fMRI BOLD contrast between the error and correct incongruent trials was also in the dACC. However, significant BOLD activation was found in the PCC for adult participants. Finally, age-related difference was confirmed by the fMRI-conditioned ERN source results.

This study has implications for two areas of research on error monitoring. First, our ERP results were consistent with studies showing increases in the amplitude of the ERN from 12 years through adulthood (Buzzell, Richards, et al., 2017; Davies et al., 2004; Gavin et al., 2019; Ladouceur et al., 2007; Lo, 2018; Overbye et al., 2019; Roe et al., 2021; Taylor et al., 2018). Lo (2018) reviewed studies showing differences in children, adolescents, and adults in the ERN and N2. The ERN may reflect post-error processing in cognitive conflict situations (Botvinick et al., 2004; Lo, 2018; van Veen & Carter, 2002b; van Veen & Carter, 2006). Thus, age differences exist in capacities engaged by error commission from early adolescence to adulthood (Lo, 2018).

Crucially, we also identified age-related differences in the scalp distribution of the ERN activity, which was centered over more frontal scalp areas in younger participants and central scalp areas in adults. This finding is in line with a prior study by Davies and colleagues (Davies et al., 2004), which found that the ERN was larger over more central locations for adults, whereas children exhibited a larger ERN over more frontal regions. Similarly, previous studies on ERN responses in children identified this component as being largest over more anterior locations (Brooker & Buss, 2014; Grammer et al., 2014; Lo, 2018). We reported a similar pattern in a prior study (Buzzell, Richards, et al., 2017) among a subset of the current sample. However, taken together with other work, the current study provides convincing evidence that the topography of the ERN differs along an anterior–posterior gradient across development. This difference in topography may arise from changes in the sources contributing to the ERN, as opposed to more simple age-related changes in a common source contributing to the ERN across ages. Our study suggests the need for more research examining how age affects error monitoring, including work comparing specific capacities engaged by error commission across the lifespan. The findings inform understanding of error monitoring development in adolescence and early adulthood, a time when significant changes occur in brain structure and function, as well as in expressions of mental health problems, such as depression and anxiety. Extensions of this work could identify neural markers of risk that manifest before clinical signs arise, providing opportunities for early intervention.

A second implication of our results refers to the source localization findings, which suggest that the location of the ERN generators may differ across age. Many scientists localize the ERN generators to the dACC (Iannaccone et al., 2015; Lo, 2018; Tamnes et al., 2013; van Veen & Carter, 2002b), which is the same location of the N2 source and commonly observed error-evoked activations
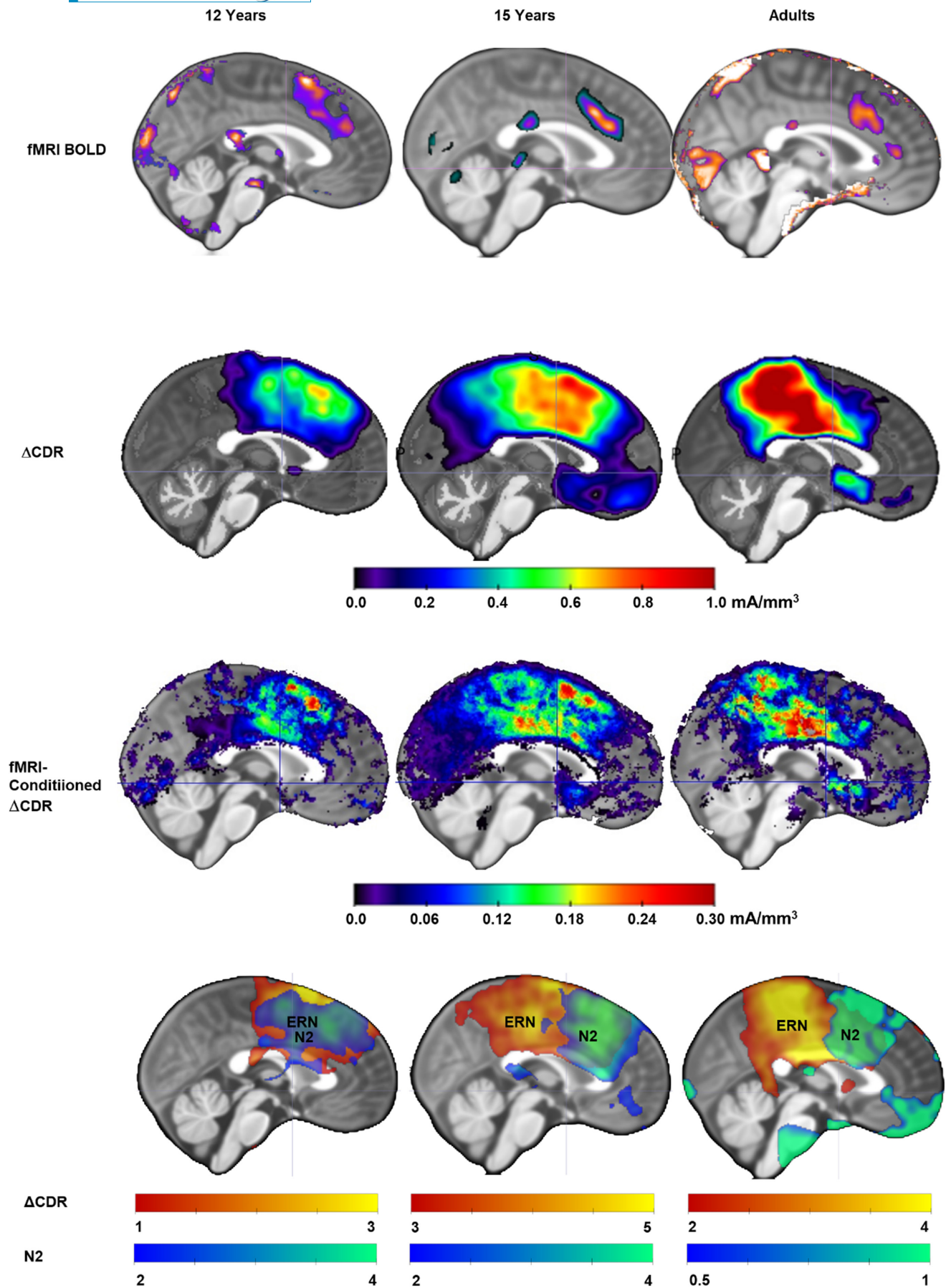
FIGURE 8 Sagittal view of the group ΔCDR activity at the peak of the response-locked ERN component (second row) overlaid on the age-specific average template, and the fMRI-conditioned ΔCDR (third row). The cross is centered to the anterior commissure of each template. The top row displays the BOLD activity for the error > correct contrast. The reconstructed source activates of both ERN and N2 components are depicted in the bottom row. Overlapping sources are evident for the 12-year-old group, whereas more posterior ERN activity occurred in adults.
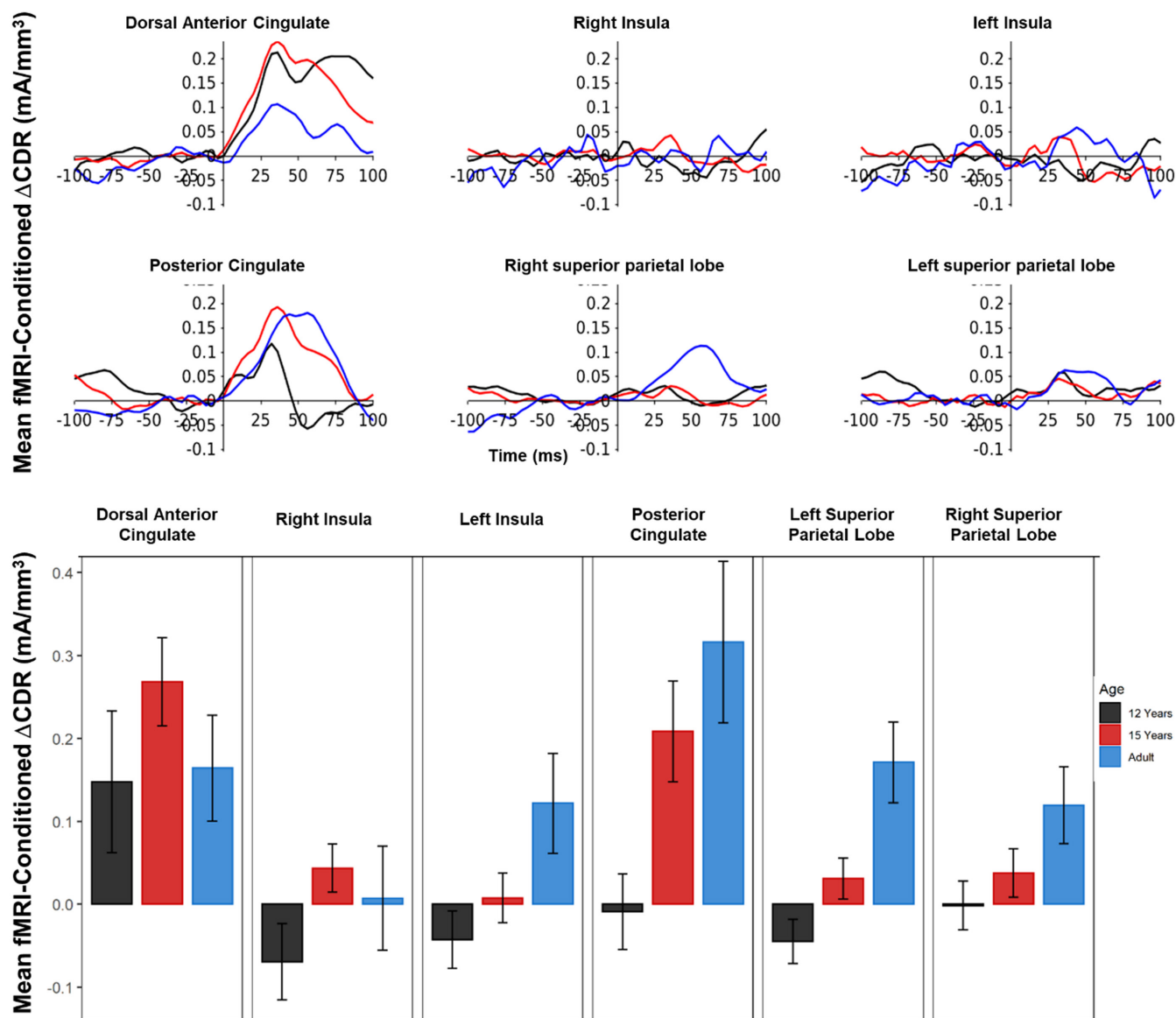

FIGURE 9 The pattern of fMRI-conditioned ΔCDR activity at the latency of the ΔERN component is depicted in the line plots for each considered ROI as a function of participant's age. Bar plots report the average fMRI-conditioned ΔCDR at the peak of the ERN activity. The largest fMRI-conditioned ΔCDR activity was localized in the dACC for the adolescent groups and more posteriorly (PCC) in adults. Raincloud plots depict the fMRI-conditioned ΔCDR activity in PCC as a function of age. Dots represent individual data points. Error bars indicate the SE from the mean.

in fMRI studies (Botvinick et al., 2004; Lo, 2018; van Veen & Carter, 2002b; van Veen & Carter, 2006). However, we found different generators for the ERN and the N2, consistent with earlier analyses on a subset of the data for the current study (Buzzell, Richards, et al., 2017), and another multimodal study (Agam et al., 2011). Posterior portions of the cingulate cortex showed activation also

in our fMRI analyses. However, a larger cluster of activity was identified across ages in more anterior areas, in line with previous neurodevelopmental studies of error monitoring (Taylor et al., 2007). Thus, fMRI-based studies identify the dACC as a central hub of the error monitoring network that comprise other cortical regions. Our results indicate some differences in the distribution of neural
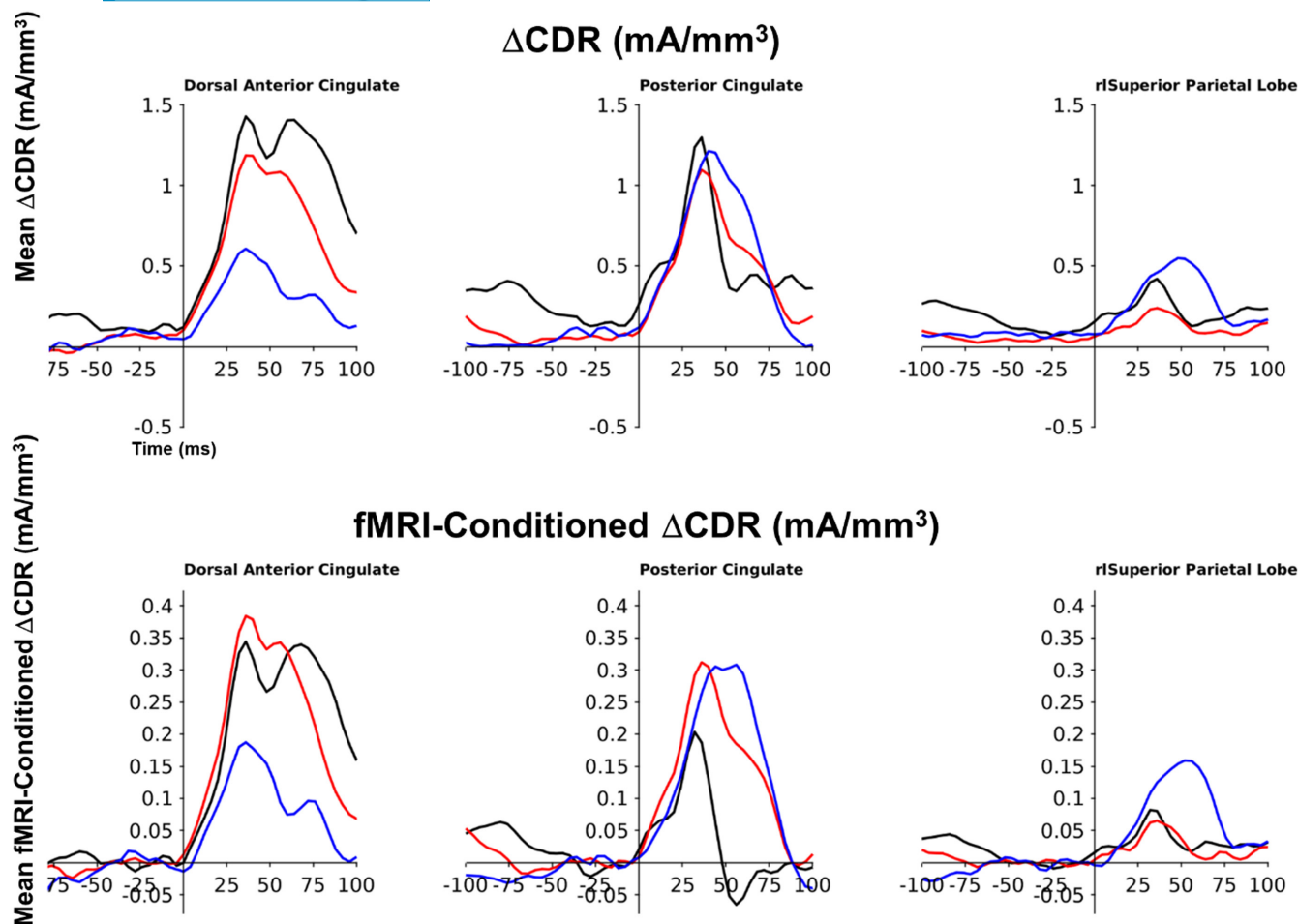
FIGURE 10 The pattern of ΔCDR and fMRI-conditioned ΔCDR activity at the latency of the ΔERN component for the two Neurosynth ROIs showing age effects, PCC and superior parietal cortex, along with the dACC.

activity across modalities, which may be due to the nature of the physiological activity intrinsic to each acquisition. Nonetheless, the availability of multi-modal acquisitions allowed us to identify where the relations between fMRI and EEG neural generators occurred.

Beyond differences in topography, our study also found differences in developmental patterns for the ERN and the N2. While age differences manifested in the source location of the ERN, the N2 source laid within the dACC at all testing ages. Consistent with such differing developmental patterns, the source of the N2 and ERN appeared to align at age 12 before diverging in adolescence and the transition to adulthood. While our results only loosely differentiate the cognitive processes unique to the N2 and the ERN, these new findings might generate interest in such processes. Of note, the N2 represents a stimulus-evoked signal, in contrast to the ERN, which is a response-evoked signal. Thus, our results differentiate development as it relates to stimulus-evoked as opposed to response-evoked cognitive processes.

Agam et al. (Agam et al., 2011) highlighted inconsistencies in previous work examining the cortical source of the ERN. Approximately half of the studies reviewed in that paper reported a source in the anterior portion of the dACC, and the remaining studies reported the source in the very posterior portion of the dACC or in the PCC. Methodological differences among studies may account for the different findings. Our study and Agam et al. (Agam et al., 2011) used realistic (MRI-constrained) models for the head and the cortical sources, contemporary methods for source analysis, and a distributed source solution. Similarity in methods may account for similar findings in the current study and Agam et al. (Agam et al., 2011). Both studies also identified comparable fMRI activations in anterior and posterior areas of the cingulate. Agam et al. (2011) report that their fMRI error activations were primarily in the dorsal region of the ACC, but also a subthreshold activation in the PCC. Comparable results were found in our current work. The largest activation on the error contrast was in the dACC and bilateral insula. However, there was also a reliable activation in the PCC at all three testing ages. It is beyond the scope of the current study to identify the specific mechanism that would explain the change from the dACC to the PCC. However,

these fMRI findings were also consistent with the Neurosynth meta-analysis. There was an increase across the testing ages in the amplitude of the ERN source in the PCC ROI. Moreover, the PCC also exhibited the largest source of activity for the ERN for the adult participants.

Our results raise questions regarding the functional role of the N2 in Flanker task performance. We found a significant but small difference between the N2 component on correct congruent and incongruent trials, with no age-related changes in the N2 amplitude, and no age changes in the congruent-incongruent differences. The difference in the N2 sources of the congruent and incongruent stimuli in the dACC region also was small (e.g., $<0.4\,\mu A/mm^3$) and nonsignificant. Thus, questions remain on the location of stimulus-evoked, conflict-specific neural processes. Some studies have examined the N2 and its cortical source in go-no-go tasks; the studies cited below use the N2b as described in the introduction. One study, using a source analysis of the difference wave (no-go minus go), localized the ERN component in the dorsal anterior cingulate at the approximate time of the N2 (Kiefer et al., 1998). However, the amplitude of the N2 was not significantly different in the go and no-go trials. This indicates that the condition difference localized in the dACC was likely recorded elsewhere on the scalp. A second study also examined the N2 in the go-no-go task (Lavric et al., 2004). This study also identified the N2b for their analysis. However, in this study the difference between the go and no-go trials did not occur on the frontal central EEG channels but on lateral frontocentral channels (e.g., C4). The LORETA source of the component was in right lateral areas rather than in the dACC. A third study also used the N2b for their go-no-go analysis (Bokura et al., 2001). The authors also report differences between the go and no-go trials in lateral scalp locations and locate the source of the components in lateral brain areas. The N2 has been studied in the flanker task, with conflicting results. Several studies reported a large N2 (N2b) response to both the congruent and incongruent trials, with the N2 amplitude being larger for the incongruent trials (Bartholow et al., 2005; Heil et al., 2012; Yeung et al., 2004). One study reported that the N2 only occurred on the incongruent trials (Kopp et al., 1996). Two studies examined the cortical source of the N2 in the dorsal anterior cingulate using a "conflict-N2" derived analysis, that is, ΔN2 (Ladouceur et al., 2007; van Veen & Carter, 2002b). However, the N2 in these two studies was not the large N2b considered in the above-mentioned studies, but rather a small negative component occurring on the upslope of the subsequent P3 (e.g., Figure 2 in van Veen & Carter, 2002a, 2002b). To the best of our knowledge, these are the only two studies using the flanker test for analyzing

the source of a ΔN2 component. No study has localized the neural generator of the N2b ERP. In a more recent publication, Kalamala and colleagues (2018) argue that when equal number of congruent and incongruent trials are presented in a basic Flanker task, the N2 component may be reflecting frontal aspects of the P300 ERP (Kałamała et al., 2018).

Our study examined the sum of the sources of the congruent and incongruent trials and found this to be in the dACC at all three testing ages. The difference in the sources of the congruent and incongruent stimuli in the dorsal anterior cingulate region were very small (e.g., $<0.4\,\mu A/mm^3$) and nonsignificant. This suggests that the difference in the ERP component derived from other brain areas (e.g., possible occipital differences). The N2 being in a similar location to the fMRI BOLD error response does not necessarily represent the same cognitive process, since the N2 analysis in our study does not come from the error/correct contrast represented by the fMRI BOLD response.

5 | CONCLUSION AND FUTURE DIRECTIONS

Overall, the results of our study speak in favor of age-related differences in the ERN amplitude and its neural generator, which covers more posterior regions with increasing age. This difference is confirmed in fMRI-constrained source analysis. It is worth noting that the interaction between age and ROI was nonsignificant. However, results of planned comparisons highlighted the role of the PCC for older participants. The multi-modality approach used in the current study allowed us to identify commonalities in the results obtained from independent acquisitions. We identified the specific regions in the fMRI activation that showed a relation with the neural generators of EEG responses. These occurred in more posterior areas for adults and anterior regions for younger participants.

Participants performed non-simultaneous EEG and fMRI acquisitions in different experimental settings. Both tasks were designed to be event-related, thus providing comparable task performances. There were differences in the behavioral performance, which was characterized by faster response times in the EEG task than the fMRI task. However, in both tasks, we observed a congruency effect, with faster responses to congruent than incongruent trials, as well as a higher accuracy and shorter response times with increasing age. It is likely that the overall difference in the speed of response between the fMRI and EEG tasks was determined by idiosyncratic features of the two experimental settings.

The inclusion of temporal information and the use of multiple neuroimaging modalities provide a better picture on the organization of neural responses involved in

performance and error monitoring. Several factors (e.g., brain maturation and functional organization, increased performance monitoring skills) may play a role in these age-related differences. Further studies are needed to characterize the mechanisms and causes determining the differences in neural organization between adolescents and adults, including the role of hormonal changes in influencing neurodevelopmental processes (Gorday & Meyer, 2018). Moreover, a fully longitudinal study could better assess developmental trends by tracking behavioral and neural responses across adolescence and early adulthood. Extending the investigation to younger children and older adults would also benefit the characterization of error processing mechanisms in stages of the lifespan in which important brain changes and variations in behavioral response to errors occur. Lastly, further investigations could extend the results of the current study by assessing how developmental changes in performance monitoring neural activity are linked to behavioral indexes of executive functioning as well as individual differences in anxiety and temperamental traits that are known to modulate the ERN activity (Cardinale et al., 2021; Meyer, 2017; Meyer, 2022; Smith et al., 2020). It is well established that the ERN activity is increased in individuals with heightened levels of anxiety (Meyer, 2017). Similarly, the ERN activity is shown to be linked to both the structural morphology (Fang et al., 2023) and functional connectivity (Gilbertson et al., 2021) of the dACC in individuals with high trait anxiety. Thus, multimodal studies could provide additional evidence on the role of dACC as a hub for the error monitoring network and how this may be modulated by anxiety traits in individuals for whom monitoring processes are particularly relevant.

AUTHOR CONTRIBUTIONS

Stefania Conte: Data curation; formal analysis; visualization; writing – original draft; writing – review and editing. **John E. Richards:** Data curation; formal analysis; funding acquisition; methodology; validation; writing – original draft; writing – review and editing. **Nathan A. Fox:** Conceptualization; funding acquisition; supervision; writing – review and editing. **Emilio A. Valadez:** Investigation; writing – review and editing. **Marco McSweeney:** Investigation; writing – review and editing. **Enda Tan:** Investigation; writing – review and editing. **Daniel S. Pine:** Conceptualization; funding acquisition; supervision; writing – review and editing. **Anderson M. Winkler:** Methodology; writing – review and editing. **Lucrezia Liuzzi:** Investigation; writing – review and editing. **Elise M. Cardinale:** Investigation; writing – review and editing. **Lauren K. White:** Conceptualization; investigation; writing – review and editing. **George A. Buzzell:** Conceptualization; investigation; writing – review and editing.

ORCID

Stefania Conte https://orcid.org/0000-0002-8249-3288

REFERENCES

Aarts, K., & Pourtois, G. (2010). Anxiety not only increases, but also alters early error-monitoring functions. *Cognitive, Affective, & Behavioral Neuroscience*, *10*(4), 479–492. https://doi.org/10.3758/CABN.10.4.479

Agam, Y., Hamalainen, M. S., Lee, A. K., Dyckman, K. A., Friedman, J. S., Isom, M., Makris, N., & Manoach, D. S. (2011). Multimodal neuroimaging dissociates hemodynamic and electrophysiological correlates of error processing. *Proceedings of the National Academy of Sciences of the United States of America*, *108*(42), 17556–17561. https://doi.org/10.1073/pnas.1103475108

Alain, C., McNeely, H. E., He, Y., Christensen, B. K., & West, R. (2002). Neurophysiological evidence of error-monitoring deficits in patients with schizophrenia. *Cerebral Cortex*, *12*(8), 840–846. https://doi.org/10.1093/cercor/12.8.840

Araki, T., Niznikiewicz, M., Kawashima, T., Nestor, P. G., Shenton, M. E., & McCarley, R. W. (2013). Disruption of function-structure coupling in brain regions sub-serving self monitoring in schizophrenia. *Schizophrenia Research*, *146*(1–3), 336–343. https://doi.org/10.1016/j.schres.2013.02.028

Bartholow, B. D., Pearson, M. A., Dickter, C. L., Sher, K. J., Fabiani, M., & Gratton, G. (2005). Strategic control and medial frontal negativity: Beyond errors and response conflict. *Psychophysiology*, *42*(1), 33–42. https://doi.org/10.1111/j.1469-8986.2005.00258.x

Boen, R., Quintana, D. S., Ladouceur, C. D., & Tamnes, C. K. (2022). Age-related differences in the error-related negativity and error positivity in children and adolescents are moderated by sample and methodological characteristics: A meta-analysis. *Psychophysiology*, *59*(6), e14003. https://doi.org/10.1111/psyp.14003

Bokura, H., Yamaguchi, S., & Kobayashi, S. (2001). Electrophysiological correlates for response inhibition in a Go/NoGo task. *Clinical Neurophysiology*, *112*(12), 2224–2232. https://doi.org/10.1016/S1388-2457(01)00691-5

Botvinick, M. M., Cohen, J. D., & Carter, C. S. (2004). Conflict monitoring and anterior cingulate cortex: An update. *Trends in Cognitive Sciences*, *8*(12), 539–546. https://doi.org/10.1016/j.tics.2004.10.003

Brooker, R. J., & Buss, K. A. (2014). Harsh parenting and fearfulness in toddlerhood interact to predict amplitudes of preschool error-related negativity. *Developmental Cognitive Neuroscience*, *9*, 148–159. https://doi.org/10.1016/j.dcn.2014.03.001

Buzzell, G. A., Morales, S., Bowers, M. E., Troller-Renfree, S. V., Chronis-Tuscano, A., Pine, D. S., Henderson, H. A., & Fox, N. A. (2021). Inhibitory control and set shifting describe different pathways from behavioral inhibition to socially anxious behavior. *Developmental Science*, *24*(1), e13040. https://doi.org/10.1111/desc.13040

Buzzell, G. A., Richards, J. E., White, L. K., Barker, T. V., Pine, D. S., & Fox, N. A. (2017). Development of the error-monitoring system from ages 9-35: Unique insight provided by MRI-constrained source localization of EEG. *NeuroImage*, *157*, 13–26. https://doi.org/10.1016/j.neuroimage.2017.05.045

Buzzell, G. A., Troller-Renfree, S. V., Barker, T. V., Bowman, L. C., Chronis-Tuscano, A., Henderson, H. A., Kagan, J., Pine, D. S., & Fox, N. A. (2017). A neurobehavioral mechanism linking behaviorally inhibited temperament and later adolescent social anxiety. *Journal of the American Academy of Child & Adolescent Psychiatry*, *56*(12), 1097–1105. https://doi.org/10.1016/j.jaac.2017.10.007

Cardinale, E. M., Bezek, J., Morales, S., Filippi, C., Smith, A. R., Haller, S., Valadez, E. A., Harrewijn, A., Phillips, D., Chronis-Tuscano, A., Brotman, M. A., Fox, N. A., Pine, D. S., Leibenluft, E., & Kircanski, K. (2021). Cross-sectional and longitudinal associations of anxiety and irritability with adolescents' neural responses to cognitive conflict. *Biological Psychiatry*, *8*, 436–444. https://doi.org/10.1016/j.bpsc.2022.03.007

Carter, C. S., Braver, T. S., Barch, D. M., Botvinick, M. M., Noll, D., & Cohen, J. D. (1998). Anterior cingulate cortex, error detection, and the online monitoring of performance. *Science*, *280*(5364), 747–749. https://doi.org/10.1126/science.280.5364.747

Clayson, P. E. (2020). Moderators of the internal consistency of error-related negativity scores: A meta-analysis of internal consistency estimates. *Psychophysiology*, *57*(8), e13583. https://doi.org/10.1111/psyp.13583

Conte, S., Richards, J., & Zimmerman, D. (2023). White matter trajectories over the lifespan. https://doi.org/10.31234/osf.io/w7qam

Conte, S., & Richards, J. E. (2022). Cortical source analysis of event-related potentials: A developmental approach. *Developmental Cognitive Neuroscience*, *54*, 101092. https://doi.org/10.1016/j.dcn.2022.101092

Davies, P. L., Segalowitz, S. J., & Gavin, W. J. (2004). Development of response-monitoring ERPs in 7- to 25-year-olds. *Developmental Neuropsychology*, *25*(3), 355–376. https://doi.org/10.1207/s15326942dn2503_6

Debnath, R., Buzzell, G. A., Morales, S., Bowers, M. E., Leach, S. C., & Fox, N. A. (2020). The Maryland analysis of developmental EEG (MADE) pipeline. *Psychophysiology*, *57*(6), e13580. https://doi.org/10.1111/psyp.13580

Dehaene, S., Posner, M. I., & Tucker, D. M. (1994). Localization of a neural system for error detection and compensation. *Psychological Science*, *5*(5), 303–305. https://doi.org/10.1111/j.1467-9280.1994.tb00630.x

Delorme, A., & Makeig, S. (2004). EEGLAB: An open source toolbox for analysis of single-trial EEG dynamics including independent component analysis. *Journal of Neuroscience Methods*, *134*(1), 9–21. https://doi.org/10.1016/j.jneumeth.2003.10.009

Donamayor, N., Heilbronner, U., & Münte, T. F. (2012). Coupling electrophysiological and hemodynamic responses to errors. *Human Brain Mapping*, *33*(7), 1621–1633. https://doi.org/10.1002/hbm.21305

Edwards, B. G., Calhoun, V. D., & Kiehl, K. A. (2012). Joint ICA of ERP and fMRI during error-monitoring. *NeuroImage*, *59*(2), 1896–1903. https://doi.org/10.1016/j.neuroimage.2011.08.088

Erickson, K. I., Ho, M. H. R., Colcombe, S. J., & Kramer, A. F. (2005). A structural equation modeling analysis of attentional control: An event-related fMRI study. *Cognitive Brain Research*, *22*(3), 349–357. https://doi.org/10.1016/j.cogbrainres.2004.09.004

Eriksen, B. A., & Eriksen, C. W. (1974). Effects of noise letters upon the identification of a target letter in a nonsearch task. *Perception & Psychophysics*, *16*(1), 143–149. https://doi.org/10.3758/BF03203267

Fang, L., Andrzejewski, J. A., & Carlson, J. M. (2023). The gray matter morphology associated with the electrophysiological response to errors in individuals with high trait anxiety. *International Journal of Psychophysiology*, *184*, 76–83. https://doi.org/10.1016/j.ijpsycho.2022.12.007

Fang, Q., & Boas, D. A. (2009). Tetrahedral mesh generation from volumetric binary and grayscale images. In *2009 IEEE international symposium on biomedical imaging: from nano to macro* (pp. 1142–1145). Ieee. https://doi.org/10.1109/ISBI.2009.5193259

Folstein, J. R., & Van Petten, C. (2008). Influence of cognitive control and mismatch on the N2 component of the ERP: A review. *Psychophysiology*, *45*(1), 152–170. https://doi.org/10.1111/j.1469-8986.2007.00602.x

Fox, N. A., Buzzell, G. A., Morales, S., Valadez, E. A., Wilson, M., & Henderson, H. A. (2021). Understanding the emergence of social anxiety in children with behavioral inhibition. *Biological Psychiatry*, *89*(7), 681–689. https://doi.org/10.1016/j.biopsych.2020.10.004

Fox, N. A., Zeytinoglu, S., Valadez, E. A., Buzzell, G. A., Morales, S., & Henderson, H. A. (2022). Annual Research Review: Developmental pathways linking early behavioral inhibition to later anxiety. *Journal of Child Psychology and Psychiatry*, *64*, 537–561. https://doi.org/10.1111/jcpp.13702

Fuhrmann, D., Knoll, L. J., & Blakemore, S. J. (2015). Adolescence as a sensitive period of brain development. *Trends in Cognitive Sciences*, *19*(10), 558–566. https://doi.org/10.1016/j.tics.2015.07.008

Gao, C., Conte, S., Richards, J. E., Xie, W., & Hanayik, T. (2019). The neural sources of N170: Understanding timing of activation in face-selective areas. *Psychophysiology*, *56*(6), e13336. https://doi.org/10.1111/psyp.13336

Gavin, W. J., Lin, M. H., & Davies, P. L. (2019). Developmental trends of performance monitoring measures in 7- to 25-year-olds: Unraveling the complex nature of brain measures. *Psychophysiology*, *56*(7), e13365. https://doi.org/10.1111/psyp.13365

Gehring, W. J., Liu, Y., Orr, J. M., & Carp, J. (2012). The error-related negativity (ERN/Ne). In *The Oxford handbook of event-related potential components* (p. 231). Oxford University Press.

Gilbertson, H., Fang, L., Andrzejewski, J. A., & Carlson, J. M. (2021). Dorsal anterior cingulate cortex intrinsic functional connectivity linked to electrocortical measures of error monitoring. *Psychophysiology*, *58*(5), e13794. https://doi.org/10.1111/psyp.13794

Giorgio, A., Watkins, K. E., Chadwick, M., James, S., Winmill, L., Douaud, G., De Stefano, N., Matthews, P. M., Smith, S. M., Johansen-Berg, H., & James, A. C. (2010). Longitudinal changes in grey and white matter during adolescence. *NeuroImage*, *49*(1), 94–103. https://doi.org/10.1016/j.neuroimage.2009.08.003

Gorday, J. Y., & Meyer, A. (2018). Linking puberty and error-monitoring: Relationships between self-reported pubertal stages, pubertal hormones, and the error-related negativity in a large sample of children and adolescents. *Developmental Psychobiology*, *60*(4), 483–490. https://doi.org/10.1002/dev.21625

Gorgolewski, K. J., Storkey, A. J., Bastin, M. E., & Pernet, C. R. (2012). Adaptive thresholding for reliable topological inference in single subject fMRI analysis [Methods]. *Frontiers in Human Neuroscience*, *6*(245), 245. https://doi.org/10.3389/fnhum.2012.00245

Grammer, J. K., Carrasco, M., Gehring, W. J., & Morrison, F. J. (2014). Age-related changes in error processing in young children: A school-based investigation. *Developmental Cognitive Neuroscience*, *9*, 93–105. https://doi.org/10.1016/j.dcn.2014.02.001

Grydeland, H., Westlye, L. T., Walhovd, K. B., & Fjell, A. M. (2016). Intracortical posterior cingulate myelin content relates to error processing: Results from T1- and T2-weighted MRI myelin mapping and electrophysiology in healthy adults. *Cerebral Cortex*, *26*, 2402–2410. https://doi.org/10.1093/cercor/bhv065

Hanayik, T., & Richards, J. E. (2018). Preprocess and processing of fMRI for faces and houses study. ResearchGate https://doi.org/10.13140/RG.2.2.36556.46722

Heil, M., Osman, A., Wiegelmann, J., Rolke, B., & Hennighausen, E. (2012). N200 in the Eriksen-task: Inhibitory executive processes? *Journal of Psychophysiology*, *14*, 218–225. https://doi.org/10.1027//0269-8803.14.4.218

Herrmann, M. J., Römmler, J., Ehlis, A.-C., Heidrich, A., & Fallgatter, A. J. (2004). Source localization (LORETA) of the error-related-negativity (ERN/Ne) and positivity (Pe). *Cognitive Brain Research*, *20*(2), 294–299. https://doi.org/10.1016/j.cogbrainres.2004.02.013

Hochman, E. Y., Eviatar, Z., Breznitz, Z., Nevat, M., & Shaul, S. (2009). Source localization of error negativity: Additional source for corrected errors. *Neuroreport*, *20*(13), 1144–1148. https://doi.org/10.1097/WNR.0b013e32832f84ed

Huynh, H. (1978). Some approximate tests for repeated measurement designs. *Psychometrika*, *43*(2), 161–175. https://doi.org/10.1007/Bf02293860

Huynh, H., & Feldt, L. S. (1980). Performance of traditional F-tests in repeated measures designs under covariance heterogeneity. *Communications in Statistics Part A-Theory and Methods*, *9*(1), 61–74. https://doi.org/10.1080/03610928008827859

Iannaccone, R., Hauser, T. U., Staempfli, P., Walitza, S., Brandeis, D., & Brem, S. (2015). Conflict monitoring and error processing: New insights from simultaneous EEG-fMRI. *NeuroImage*, *105*, 395–407. https://doi.org/10.1016/j.neuroimage.2014.10.028

Jenkinson, M., Bannister, P., Brady, M., & Smith, S. (2002). Improved optimization for the robust and accurate linear registration and motion correction of brain images. *NeuroImage*, *17*(2), 825–841. https://doi.org/10.1016/s1053-8119(02)91132-8

Jenkinson, M., & Smith, S. (2001). A global optimisation method for robust affine registration of brain images. *Medical Image Analysis*, *5*(2), 143–156. https://doi.org/10.1016/s1361-8415(01)00036-6

Jurcak, V., Tsuzuki, D., & Dan, I. (2007). 10/20, 10/10, and 10/5 systems revisited: Their validity as relative head-surface-based positioning systems. *NeuroImage*, *34*(4), 1600–1611. https://doi.org/10.1016/j.neuroimage.2006.09.024

Kałamała, P., Szewczyk, J., Senderecka, M., & Wodniecka, Z. (2018). Flanker task with equiprobable congruent and incongruent conditions does not elicit the conflict N2. *Psychophysiology*, *55*(2), e12980. https://doi.org/10.1111/psyp.12980

Kiefer, M., Marzinzik, F., Weisbrod, M., Scherg, M., & Spitzer, M. (1998). The time course of brain activations during response inhibition: Evidence from event-related potentials in a go/no go task. *Neuroreport*, *9*, 765–770.

Kopp, B., Rist, F., & Mattler, U. (1996). N200 in the flanker task as a neurobehavioral tool for investigating executive control. *Psychophysiology*, *33*(3), 282–294. https://doi.org/10.1111/j.1469-8986.1996.tb00425.x

Ladouceur, C. D., Dahl, R. E., & Carter, C. S. (2007). Development of action monitoring through adolescence into adulthood: ERP and source localization. *Developmental Science*, *10*(6), 874–891. https://doi.org/10.1111/j.1467-7687.2007.00639.x

Lavric, A., Pizzagalli, D. A., & Forstmeier, S. (2004). When 'go' and 'nogo' are equally frequent: ERP components and cortical tomography. *European Journal of Neuroscience*, *20*(9), 2483–2488. https://doi.org/10.1111/j.1460-9568.2004.03683.x

Le, T. M., Potvin, S., Zhornitsky, S., & Li, C.-S. R. (2021). Distinct patterns of prefrontal cortical disengagement during inhibitory control in addiction: A meta-analysis based on population characteristics. *Neuroscience & Biobehavioral Reviews*, *127*, 255–269. https://doi.org/10.1016/j.neubiorev.2021.04.028

Leach, S. C., Morales, S., Bowers, M. E., Buzzell, G. A., Debnath, R., Beall, D., & Fox, N. A. (2020). Adjusting ADJUST: Optimizing the ADJUST algorithm for pediatric data using geodesic nets. *Psychophysiology*, *57*(8), e13566. https://doi.org/10.1111/psyp.13566

Lecoutre, B. (1991). A correction for the epsilon-approximately approximate test in repeated measures designs with 2 or more independent groups. *Journal of Educational Statistics*, *16*(4), 371–372. https://doi.org/10.2307/1165108

Lo, S. L. (2018). A meta-analytic review of the event-related potentials (ERN and N2) in childhood and adolescence: Providing a developmental perspective on the conflict monitoring theory. *Developmental Review*, *48*, 82–112. https://doi.org/10.1016/j.dr.2018.03.005

Lopez-Calderon, J., & Luck, S. J. (2014). ERPLAB: An open-source toolbox for the analysis of event-related potentials. *Frontiers in Human Neuroscience*, *8*, 213. https://doi.org/10.3389/fnhum.2014.00213

MacDonald, A. W., Cohen, J. D., Stenger, V. A., & Carter, C. S. (2000). Dissociating the role of the dorsolateral prefrontal and anterior cingulate cortex in cognitive control. *Science*, *288*(5472), 1835–1838. https://doi.org/10.1126/science.288.5472.1835

Mathewson, K. J., Dywan, J., & Segalowitz, S. J. (2005). Brain bases of error-related ERPs as influenced by age and task. *Biological Psychology*, *70*(2), 88–104. https://doi.org/10.1016/j.biopsycho.2004.12.005

Mehra, L. M., Hajcak, G., & Meyer, A. (2022). The relationship between stressful life events and the error-related negativity in children and adolescents. *Developmental Cognitive Neuroscience*, *55*, 101110. https://doi.org/10.1016/j.dcn.2022.101110

Meyer, A. (2017). A biomarker of anxiety in children and adolescents: A review focusing on the error-related negativity (ERN) and anxiety across development. *Developmental Cognitive Neuroscience*, *27*, 58–68. https://doi.org/10.1016/j.dcn.2017.08.001

Meyer, A. (2022). On the relationship between the error-related negativity and anxiety in children and adolescents: From a neural marker to a novel target for intervention. *Psychophysiology*, *59*(6), e14050. https://doi.org/10.1111/psyp.14050

Meyer, A., Nelson, B., Perlman, G., Klein, D. N., & Kotov, R. (2018). A neural biomarker, the error-related negativity, predicts the first onset of generalized anxiety disorder in a large sample of adolescent females. *Journal of Child Psychology and Psychiatry*, *59*(11), 1162–1170. https://doi.org/10.1111/jcpp.12922

Meyer, A., Riesel, A., & Proudfit, G. H. (2013). Reliability of the ERN across multiple tasks as a function of increasing errors. *Psychophysiology*, *50*(12), 1220–1225. https://doi.org/10.1111/psyp.12132

Michel, C. M., Murray, M. M., Lantz, G., Gonzalez, S., Spinelli, L., & Grave de Peralta, R. (2004). EEG source imaging. *Clinical Neurophysiology*, *115*(10), 2195–2222. https://doi.org/10.1016/j.clinph.2004.06.001

Mognon, A., Jovicich, J., Bruzzone, L., & Buiatti, M. (2011). ADJUST: An automatic EEG artifact detector based on the joint use of spatial and temporal features. *Psychophysiology*, *48*(2), 229–240. https://doi.org/10.1111/j.1469-8986.2010.01061.x

Moser, J. S., Moran, T. P., Schroder, H. S., Donnellan, M. B., & Yeung, N. (2013). On the relationship between anxiety and error monitoring: A meta-analysis and conceptual framework. *Frontiers in Human Neuroscience*, *7*, 466. https://doi.org/10.3389/fnhum.2013.00466

Munro, G. E., Dywan, J., Harris, G. T., McKee, S., Unsal, A., & Segalowitz, S. J. (2007). ERN varies with degree of psychopathy in an emotion discrimination task. *Biological Psychology*, *76*(1–2), 31–42. https://doi.org/10.1016/j.biopsycho.2007.05.004

Nee, D. E., Wager, T. D., & Jonides, J. (2007). Interference resolution: Insights from a meta-analysis of neuroimaging tasks. *Cognitive, Affective, & Behavioral Neuroscience*, *7*(1), 1–17. https://doi.org/10.3758/CABN.7.1.1

Nolan, H., Whelan, R., & Reilly, R. B. (2010). FASTER: Fully automated statistical thresholding for EEG artifact rejection. *Journal of Neuroscience Methods*, *192*(1), 152–162. https://doi.org/10.1016/j.jneumeth.2010.07.015

Norbom, L. B., Ferschmann, L., Parker, N., Agartz, I., Andreassen, O. A., Paus, T., Westlye, L. T., & Tamnes, C. K. (2021). New insights into the dynamic development of the cerebral cortex in childhood and adolescence: Integrating macro-and microstructural MRI findings. *Progress in Neurobiology*, *204*, 102109. https://doi.org/10.1016/j.pneurobio.2021.102109

O'Connell, R. G., Dockree, P. M., Bellgrove, M. A., Kelly, S. P., Hester, R., Garavan, H., Robertson, I. H., & Foxe, J. J. (2007). The role of cingulate cortex in the detection of errors with and without awareness: A high-density electrical mapping study. *The European Journal of Neuroscience*, *25*(8), 2571–2579. https://doi.org/10.1111/j.1460-9568.2007.05477.x

Oostenveld, R., Fries, P., Maris, E., & Schoffelen, J. M. (2011). FieldTrip: Open source software for advanced analysis of MEG, EEG, and invasive electrophysiological data. *Computational Intelligence and Neuroscience*, *2011*, 156869. https://doi.org/10.1155/2011/156869

Overbye, K., Walhovd, K. B., Paus, T., Fjell, A. M., Huster, R. J., & Tamnes, C. K. (2019). Error processing in the adolescent brain: Age-related differences in electrophysiology, behavioral adaptation, and brain morphology. *Developmental Cognitive Neuroscience*, *38*, 100665. https://doi.org/10.1016/j.dcn.2019.100665

Pascual-Marqui, R. D., Lehmann, D., Koukkou, M., Kochi, K., Anderer, P., Saletu, B., Tanaka, H., Hirata, K., John, E. R., Prichep, L., Biscay-Lirio, R., & Kinoshita, T. (2011). Assessing interactions in the brain with exact low-resolution electromagnetic tomography. *Transactions of the Royal Society A: Mathematical, Physical and Engineering Sciences*, *369*(1952), 3768–3784. https://doi.org/10.1098/rsta.2011.0081

Pascual-Marqui, R. D., Pascual-Montano, A. D., Lehmann, D., Kochi, K., Esslen, M., Jancke, L., Anderer, P., Saletu, B., Tanaka, H., Hirata, K., John, E. R., & Prichep, L. (2006). Exact low resolution brain electromagnetic tomography (eLORETA). *NeuroImage*, *31*(Suppl. 1), S86.

Richards, J. E., Boswell, C., Stevens, M., & Vendemia, J. M. (2015). Evaluating methods for constructing average high-density electrode positions. *Brain Topography*, *28*(1), 70–86. https://doi.org/10.1007/s10548-014-0400-8

Richards, J. E., Sanchez, C., Phillips-Meek, M., & Xie, W. (2016). A database of age-appropriate average MRI templates. *NeuroImage*, *124*(Pt B), 1254–1259. https://doi.org/10.1016/j.neuroimage.2015.04.055

Richards, J. E., & Xie, W. (2015). Brains for all the ages: Structural neurodevelopment in infants and children from a life-span perspective. In J. Benson (Ed.), *Advances in Child Development and Behavior* (Vol. 48, pp. 1–52). Elsevier. https://doi.org/10.1016/bs.acdb.2014.11.001

Ridderinkhof, K. R., Ullsperger, M., Crone, E. A., & Nieuwenhuis, S. (2004). The role of the medial frontal cortex in cognitive control. *Science*, *306*(5695), 443–447. https://doi.org/10.1126/science.1100301

Roe, M. A., Engelhardt, L. E., Nugiel, T., Harden, K. P., Tucker-Drob, E. M., & Church, J. A. (2021). Error-signaling in the developing brain. *NeuroImage*, *227*, 117621. https://doi.org/10.1016/j.neuroimage.2020.117621

Santesso, D. L., & Segalowitz, S. J. (2008). Developmental differences in error-related ERPs in middle- to late-adolescent males. *Developmental Psychology*, *44*(1), 205–217. https://doi.org/10.1037/0012-1649.44.1.205

Segalowitz, S. J., Santesso, D. L., Murphy, T. I., Homan, D., Chantziantoniou, D. K., & Khan, S. (2010). Retest reliability of medial frontal negativities during performance monitoring. *Psychophysiology*, *47*(2), 260–270. https://doi.org/10.1111/j.1469-8986.2009.00942.x

Smith, A. R., White, L. K., Leibenluft, E., McGlade, A. L., Heckelman, A. C., Haller, S. P., Buzzell, G. A., Fox, N. A., & Pine, D. S. (2020). The heterogeneity of anxious phenotypes: Neural responses to errors in treatment-seeking anxious and behaviorally inhibited youths. *Journal of the American Academy of Child and Adolescent Psychiatry*, *59*(6), 759–769. https://doi.org/10.1016/j.jaac.2019.05.014

Sydnor, V. J., Larsen, B., Bassett, D. S., Alexander-Bloch, A., Fair, D. A., Liston, C., Mackey, A. P., Milham, M. P., Pines, A., Roalf, D. R., Seidlitz, J., Xu, T., Raznahan, A., & Satterthwaite, T. D. (2021). Neurodevelopment of the association cortices: Patterns, mechanisms, and implications for psychopathology. *Neuron*, *109*(18), 2820–2846. https://doi.org/10.1016/j.neuron.2021.06.016

Tamnes, C. K., Walhovd, K. B., Torstveit, M., Sells, V. T., & Fjell, A. M. (2013). Performance monitoring in children and adolescents: A review of developmental changes in the error-related negativity and brain maturation. *Developmental Cognitive Neuroscience*, *6*, 1–13. https://doi.org/10.1016/j.dcn.2013.05.001

Tang, A., Crawford, H., Morales, S., Degnan, K. A., Pine, D. S., & Fox, N. A. (2020). Infant behavioral inhibition predicts personality and social outcomes three decades later. *Proceedings of the National Academy of Sciences*, *117*(18), 9800–9807. https://doi.org/10.1073/pnas.1917376117

Taylor, J. B., Visser, T. A. W., Fueggle, S. N., Bellgrove, M. A., & Fox, A. M. (2018). The error-related negativity (ERN) is an electrophysiological marker of motor impulsiveness on the Barratt Impulsiveness Scale (BIS-11) during adolescence. *Developmental Cognitive Neuroscience*, *30*, 77–86. https://doi.org/10.1016/j.dcn.2018.01.003

Taylor, S. F., Stern, E. R., & Gehring, W. J. (2007). Neural systems for error monitoring: Recent findings and theoretical perspectives. *The Neuroscientist*, *13*(2), 160–172. https://doi.org/10.1177/1073858406298184

Tran, A. P., Yan, S., & Fang, Q. (2020). Improving model-based functional near-infrared spectroscopy analysis using mesh-based anatomical and light-transport models. *Neurophotonics*, *7*(1), 015008. https://doi.org/10.1117/1.NPh.7.1.015008

van Veen, V., & Carter, C. S. (2002a). The anterior cingulate as a conflict monitor: fMRI and ERP studies. *Physiology & Behavior*, *77*(4–5), 477–482. https://doi.org/10.1016/s0031-9384(02)00930-7

van Veen, V., & Carter, C. S. (2002b). The timing of action-monitoring processes in the anterior cingulate cortex. *Journal of Cognitive Neuroscience*, *14*(4), 593–602. https://doi.org/10.1162/08989290260045837

van Veen, V., & Carter, C. S. (2006). Error detection, correction, and prevention in the brain: A brief review of data and theories. *Clinical EEG and Neuroscience*, *37*(4), 330–335. https://doi.org/10.1177/155005940603700411

van Veen, V., Cohen, J. D., Botvinick, M. M., Stenger, V. A., & Carter, C. S. (2001). Anterior cingulate cortex, conflict monitoring, and levels of processing. *NeuroImage*, *14*(6), 1302–1308. https://doi.org/10.1006/nimg.2001.0923

vel Grajewska, B. Ż., Sim, E. J., Hoenig, K., Herrnberger, B., & Kiefer, M. (2011). Mechanisms underlying flexible adaptation of cognitive control: Behavioral and neuroimaging evidence in a flanker task. *Brain Research*, *1421*, 52–65. https://doi.org/10.1016/j.brainres.2011.09.022

Vlamings, P. H., Jonkman, L. M., Hoeksma, M. R., van Engeland, H., & Kemner, C. (2008). Reduced error monitoring in children with autism spectrum disorder: An ERP study. *The European Journal of Neuroscience*, *28*(2), 399–406. https://doi.org/10.1111/j.1460-9568.2008.06336.x

Vocat, R., Pourtois, G., & Vuilleumier, P. (2008). Unavoidable errors: A spatio-temporal analysis of time-course and neural sources of evoked potentials associated with error processing in a speeded task. *Neuropsychologia*, *46*(10), 2545–2555. https://doi.org/10.1016/j.neuropsychologia.2008.04.006

Vorwerk, J., Cho, J. H., Rampp, S., Hamer, H., Knosche, T. R., & Wolters, C. H. (2014). A guideline for head volume conductor modeling in EEG and MEG. *NeuroImage*, *100*, 590–607. https://doi.org/10.1016/j.neuroimage.2014.06.040

Vorwerk, J., Hanrath, A., Wolters, C. H., & Grasedyck, L. (2019). The multipole approach for EEG forward modeling using the finite element method. *NeuroImage*, *201*, 116039. https://doi.org/10.1016/j.neuroimage.2019.116039

Vorwerk, J., Magyari, L., Ludewig, J., Oostenveld, R., & Wolters, C. H. (2013). The fieldtrip-simbio pipeline for finite element EEG forward computations in MATLAB: Validation and application. In The International Conference on Basic and Clinical Multimodal Imaging, Geneva, Switzerland.

Weinberg, A., Riesel, A., & Hajcak, G. (2012). Integrating multiple perspectives on error-related brain activity: The ERN as a neural indicator of trait defensive reactivity. *Motivation and Emotion*, *36*, 84–100. https://doi.org/10.1007/s11031-011-9269-y

Weiss, H., & Luciana, M. (2022). Neurobehavioral maturation of motor response inhibition in adolescence—A narrative review. *Neuroscience & Biobehavioral Reviews*, *137*, 104646. https://doi.org/10.1016/j.neubiorev.2022.104646

Westlye, L. T., Walhovd, K. B., Bjørnerud, A., Due-Tønnessen, P., & Fjell, A. M. (2009). Error-related negativity is mediated by fractional anisotropy in the posterior cingulate gyrus—A study combining diffusion tensor imaging and electrophysiology in healthy adults. *Cerebral Cortex*, *19*(2), 293–304. https://doi.org/10.1093/cercor/bhn084

Winkler, A. M., Ridgway, G. R., Webster, M. A., Smith, S. M., & Nichols, T. E. (2014). Permutation inference for the general linear model. *NeuroImage*, *92*(100), 381–397. https://doi.org/10.1016/j.neuroimage.2014.01.060

Wittfoth, M., Küstermann, E., Fahle, M., & Herrmann, M. (2008). The influence of response conflict on error processing: Evidence from event-related fMRI. *Brain Research*, *1194*, 118–129. https://doi.org/10.1016/j.brainres.2007.11.067

Yarkoni, T., Poldrack, R. A., Nichols, T. E., Van Essen, D. C., & Wager, T. D. (2011). Large-scale automated synthesis of human functional neuroimaging data. *Nature Methods*, *8*(8), 665–670. https://doi.org/10.1038/nmeth.1635

Yeung, N., Botvinick, M. M., & Cohen, J. D. (2004). The neural basis of error detection: Conflict monitoring and the error-related negativity. *Psychological Review*, *111*(4), 931–959. https://doi.org/10.1037/0033-295X.111.4.931

Yeung, N., & Summerfield, C. (2012). Metacognition in human decision-making: Confidence and error monitoring. *Philosophical Transactions of the Royal Society of London. Series B, Biological Sciences*, *367*(1594), 1310–1321. https://doi.org/10.1098/rstb.2011.0416

SUPPORTING INFORMATION

Additional supporting information can be found online in the Supporting Information section at the end of this article.

Data S1